CHAPTER VIII

EXPLORING INCLUSION COMPLEXES OF CYCLODEXTRIN MOLECULES WITH A SIGNIFICANT COMPOUND FOR REGULATORY DISCHARGEMENT BY PHYSICOCHEMICAL CONTRIVANCE

8.1. Introduction

Uric acid is end-product of the purine catabolic path. Enzyme xanthine oxido reductase is concerned in formation of uric acid from hypoxanthine and xanthine. Xanthine oxidoreductase exists in two distinct functional forms including xanthine dehydrogenase and xanthine oxidase. [1-7]. Allopurinol or 1, 5-dihydro-4H-pyrazolo[3, 4-d] pyrimidin-4-one, is a purine inhibitor of the enzyme xanthine oxidase. This material as a significant drug for hyperuricemia can inhibit the synthesis of uric acid. [8-11]. Ever since 50 years ago, it has been administered for treatment of gout. In the year of 1946, allopurinol was developed by Elion and colleagues, at Burroughs-Wellcome Company. Allopurinol (ALP) is quickly oxidized by xanthine oxidase to hypoxanthine and xanthine, respectively. ALP after oral administration is rapidly absorbed and has a short half-life in plasma (about 2-3 hours). Therefore we have used all the supramolecular molecules with various cavity sizes to show its controlled release and increase its longevity in the plasma. Xanthine oxidase is a noteworthy biological source of free radical generation and ALP, as an antioxidant, has direct and indirect antioxidant activity on these free radicals. Furthermore, it can scavenge free radicals such as hydroxyl radical and superoxide anion and numerous studies have shown these effects of ALP. This drug revealed advantageous effects in the treatment of some renal disorders both in experimental and clinical trials. [12-17].

Macrocyclic cyclodextrins (enzymic conversion products of starch) were exposed in 1891, and structures were elucidated in the mid-1930s. Their industrial implication become obvious in the 1970s, by now thousands of tons of the three cyclodextrins (α-, β-, and HP-β-CD) and of their chemical derivatives and inclusion complexes are produced industrially. Outer surface of these doughnut-shaped molecules is hydrophilic, but they have an axial open cavity, which is of hydrophobic character and capable of including other apolar molecules (or their moiety) in case of geometric compatibility. This is the essence of molecular encapsulation by inclusion complex formation. Taking into account that one, and probably largest, field of practical utilization of CDs is based on their solubilizing capacity (mainly in pharmaceutical industry) due attention must be paid to the above-mentioned, and many other CD-related, apparent anomalies by solution chemistry.[18-25]

The goal of this paper is to give comprehensive information about therapeutic effects and the controlled delivery of allopurinol as an antioxidant agent in some diseases including hyperuricemia, renal IRI, nephrotoxicity, gout, contrast-induced nephropathy etc.

8.2. Experimental section

8.2.1 Source and purity of materials

Allopurinol and CD's purchased from Sigma-Aldrich. Mass fractions purity of both was ≥0.99. Reagents were always placed in the desiccators over P_2O_5 to keep them in dry atmosphere. These chemicals were used as received without extra purification (Scheme 1). The provenance and purity of the chemical used has been depicted in table 1.

8.2.2 Apparatus and procedure

Prior to start of the experimental work we observed that allopurinol soluble in all proportion of aqueous CD solutions. Therefore mother solutions of Allopurinol were prepared by mass (Mettler Toledo AG-285 with uncertainty 0.0003g) and then the working solutions were prepared by mass dilution.

Conversions of molarity into molality had been done using experimental density values of respective solutions and adequate precautions were taken to reduce evaporation losses during mixing in the experiment.

^{1}H NMR and 2D ROESY spectra of the solid inclusion complex prepared were recorded in D_2O using Bruker AVANCE 400 MHz instrument. The signals are presented in ppm using residual protonated solvent signal at 4.79ppm in D_2O as internal standard and all the Data are reported as chemical shift.

UV–visible spectroscopic data was carried out using JASCO V-530 UV/VIS Spectro-photometer with wavelength accuracy of ±0.5nm. Spectra were recorded at (297.15±1)K.

FTIR spectra's of solid ICs were recorded by Perkin Elmer FT-IR Spectrometer using KBr desk procedure with scanning range of 200 to 4000 cm^{-1}.

Mass Spectroscopic study was taken by JEOL GC MATE II quadruple double focusing mass analyser using electron impact ionization.

8.2.3. Preparation of Solid Inclusion Complex:

Preparations of solid inclusion complex 1.34g of CD's were dissolved in 30 ml of triply distilled and degassed water in round bottom flasks. Mixture was stirred to make homogeneous solutions over magnetic stirrer. Alternatively solutions of [ALP] was prepared taking 0.295g of [ALP] in a separate beaker with 15ml water and stirred until homogeneous mixtures were formed. Subsequent to both the homogeneous mixtures are prepared, the ALP solution was then added into CD solution slowly with continuous stirring and after completion of the addition the ALP solution the mixture was stirred for 48 h continuously. Following completion of 48 hours, mixture was allowed to cool at lower temperature when a white solid was observed. Then the precipitate was filtered and washed for several times. Lastly, the dry white powder was obtained after drying in oven at 50 °C for 24 h. The solid inclusion complex with all CD's was prepared following the same procedure. The resulting solids of inclusion complex between ALP and CD were found to dissolve in pure distilled water freely. These solids were

further analyzed and characterized by means of FTIR, UV-VIS, NMR and ESI-Mass spectroscopic methods.

8.3. Result and discussion:

The experimental physical parameter of mixtures in different mass fractions of ALP solutions at diverse temperatures.

8.3.1. JOB Plot:

Job's continuous variation method was applied to determine stoichiometry of the inclusion complexes formed. By the measurement of absorbance of a set of solutions prepared of the ALP and CD in water mixture in the mole fraction range of 0–1 (Tables 1, 2, and 3). Here we calculate (ΔA × R) values against R, where ΔA signifies the difference in absorbance of ALP in the pure form and complexed form and R is [ALP]/ ([ALP] + [CD]). λ_{max} was found at 250 nm at 298.15 K. Ratio of guest and host i.e., stoichiometry is obtained from value of R at maxima on the Job' Plot such as R ≈ 0.33, for 1:2 IC, R≈ 0.5 for 1:1 IC, R≈ 0.66 for 2:1 IC etc. In the experiment of ALP and CD's the maxima in the Job' plots were obtained at R ≈ 0.5 which is the indication of 1:1 stoichiometry of ALP and CD ICs (Figure 1a,1b and 1c).[26]

8.3.1. Determination of binding (or association) constant by UV–Vis spectroscopy

The binding constant between α-CD, β-CD, HP-β-CD and ALP has been evaluated via UV–Vis spectroscopy. The Benesi–Hildebrand technique represents one of the most common strategies to determine binding constants based on absorption spectra for inclusion complex. With the help of Benesi–Hildebrand method for 1:1 host–guest ICs, double-reciprocal plots of $1/\Delta A$ against $1/[CD]$ were plotted using the following equation (Figure 2(a, b, c), 3(a, b, c), 4(a, b, c)).

$$\frac{1}{\Delta A} = \frac{1}{\Delta\varepsilon[V]K_a} X \frac{1}{[CD]} + \frac{1}{\Delta\varepsilon[V]} \qquad \text{(VIII.1)}$$

Association constants (K_a^c) were also calculated for the inclusion complexation of ALP and CD by means of conductivity study with the help of a nonlinear program. Basing upon the fact that the insertion of the ALP inside the CD cavity changes the conductivity of the solutions. The equilibrium between ALP and CD can be represented as:

$$\text{ALP} + \text{CD} \xleftrightarrow{K_a} \text{IC} \qquad \text{(VIII.2)}$$

The equilibrium constant, K_a is represented as,

$$K_a = [IC] / [ALP][CD] * f(IC)/f(ALP)\, f(CD) \qquad \text{(VIII.3)}$$

Where, [IC], [ALP] and [CD] are molar concentrations of inclusion complex, allopurinol and cyclodextrin's at equilibrium accordingly. (f) is activity coefficients of the respective species (Table 4, 5, 6). The activity coefficient of CD, f (CD), can be assumed as unity as system was dilute. In order to have an accurate estimation of binding constants of the inclusion complexes under investigation, changes in the absorption intensity of the ALP at different wavelength, were monitored as a function of the CD's concentration and non-linear regression estimation of the K_a was chosen.

8. 3.3. FTIR:

FT-IR study of the solid ICs formed was performed to investigate the formation of the solid ICs. There are changes in frequencies of bands of the inserted guest molecules as well as some bands are absent in the spectra of complex. This may be due to the formation of the ICs. Data for pure compounds and inclusion complexes are recorded in TableS7 and spectroscopic change in wave number before and after inclusion are shown in [Figure 5(a), (b), (c), (d)]. Due to non-covalent interactions the changes of bands are observed. In the spectra of α-CD, β-CD and HP-β-CD the broad band's obtained at 3410 cm^{-1}, 3408 cm^{-1} and 3415.82 cm^{-1} are due to the valence vibrations of -O-H groups linked by H-bond. The O-H stretching for α-CD and β-CD obtained at 3410 cm^{-1} 3408 cm^{-1} and 3415.82 cm^{-1} were obtained in the complexes 3410.85 cm^{-1}, 3415.94 cm^{-1} and 3414.44 cm^{-1} respectively, may be due to the interaction of the positively

charged nitrogen atom of the pyrazole ring and the oxygen atom of (C=O) group which is again reflected in the shifted band of C=N stretching for 1701.40 cm^{-1} for the pure ALP to 1601.17 cm^{-1} in IC of α-CD, 1623.67 cm^{-1} in IC of β-CD and 1626.80 cm-1 in IC of HP-β-CD respectively. The C-H stretching and bending are obtained at 2941cm^{-1} and 1404 cm^{-1} for pure β-CD and 2919. 19 cm^{-1} and 1366.67 cm^{-1} and HP-β-CD shift is almost the same. For pure α-CD, which are shifted in the ICs to 2886.26 cm^{-1} from 2927 cm^{-1}, 1367 cm^{-1} for α-CD. The out of plane C-H bending for [ALP] obtained at 814 cm^{-1} and 768 cm^{-1} for α-CD, 761cm^{-1} for β-CD and 762 cm^{-1} for HP-β-CD respectively. This may be due to the closeness of C-H of CD and the aromatic C-H of the ALP. The aromatic stretching bands for pure [ALP] observed at 3165 cm^{-1}, stretching band due to alkyl C-H at 3081cm^{-1} and 3042 cm^{-1}, are absent in the spectra of ICs. The peak due to stretching of C-H from -CH_2- at 2941 cm^{-1} for [ALP] are absent or shifted to 2886 cm^{-1}, 2919 cm^{-1} and 2927cm^{-1}, 2922 cm^{-1} in the spectra of ICs of α-CD, β-CD and HP-β-CD respectively, may be due to interaction inside the cavity of cyclodextrin. In ICs no additional signal is obtained which deny the chance of chemical reaction. Thus the study provides major information about the formation of the ICs in the solid state. [27].

8.3.4.1. H-NMR spectroscopy

NMR spectroscopic study in aqueous solution at 298.15K. Figure 6(a), (b), (c) represents 1H NMR spectra of the complex of ALP with α-CD, β-CD and HP-β-CD which describes slight downfield shift of the aliphatic protons of guest molecule. The signal due to aryl protons are nearly shifted and little broadening. On the other hand the protons of guest molecules of the aliphatic chain show a slight change of the in their signals while present in the complex (α, β and γ protons of free ALP appears downfield shift respectively, then complex. This result clearly reveals the existence of some sort of association between the electron rich oxygen atoms of the CD's and the nitrogen atom (scheme 2). The aromatic part of the ALP shows no change of their signals indicating their free state in the solvent medium.

Upon inclusion, upfield chemical shift values (Δδ) of the H3 and H5 protons of **α** and β-Cyclodextrins and H3 protons for HP-β-CD have been shown in Figure,

which confirm that the interaction of the guest ALP with H3 is greater than that with H5, signifying that the inclusion has taken place through the wider rim of the α, β and HP-β-Cyclodextrins.

It is to be mentioned that upon inclusion some non aromatic peak of the ALP was completely disappeared in the proton NMR spectra of ALP, leave strong evidence of inclusion complexation.[28]

8.3.4. **2D-ROESY spectroscopy**

The principle of '2D ROESY' is the interaction of protons which are present in close proximity of 0.4 nm range to each other to produce NMR cross peak. In our study, we investigated the inclusion of ALP inside the α-CD, β-CD, and HP-β-CD hydrophobic cavity. NMR study was carried out in D_2O. It is clear H-3 and H-5 protons of CDs are present inside the cavity and hence if inclusion happens, there should be presence of such close proximity of 0.4 nm of the ALP protons with H-3 and H-5 protons of CD which can produce rotating-frame nuclear overhauser effect spectroscopy (ROESY) to give cross peaks.

In the Figure 7 (a), (b), (c) there is the presence of cross peaks of H3 and H5 protons of β-CD with H-3 and H-5 protons of the aromatic ring and H-4' protons of [ALP] ; with the H3 and H5 protons of α-CD and H-1', H-1"and H-4'of [ALP] and negligible cross peaks in HP-β-CD. In the dynamic process of inclusion the cross peaks are generated due to insertion of the pyrazole part of the ALP as well as the aromatic ring of the ALP but it is sterically unfavourable. Hence in some cases benzylic part and in some cases pyrazole enters inside the cavity. This signifies inclusion phenomena of the said ALP into CD cavity. [29]

8.3.4. SEM

A very illustrious technique for analyzing the surface texture and particle size of solid materials. The exterior surface morphological structures of (α- , β-, HP-β-) CD and solid IC (ALP: α-CD, ALP: β-CD, ALP: HP-β-CD) are shown in respectively. From (Figure 8 (a), (b), (c), (d)) it is obvious that morphological structures of each are totally different from each other. Moreover as the complexation by α-, β- and HP-β-CD can be viewed distinctly. This provides clear evidence that [ALP]

fits adequately into the hydrophobic cavity of CD's to figure solid IC with different morphology.[28]

8.3.4. Fluorescence

Fluorescence was extensively studied for static and dynamic properties of the aggregated system such as the derivatives of the drug. In amphiphile molecules, CD's (quencher) are preferentially solubilized in their core hydrophobic regions. Change in the microenvironment of solution is experienced by (ALP), where the shift in the absorbance is located. Hence is used to aggregate properties in the form of inclusion. Vibronic band spectra endure major perturbation on transferring from non-polar to a polar environment. Fluorescence measurements are used to determine the association and complexation, of studied complex and also in understanding interaction between the host-guest inclusion processes (ICs). Steady-state fluorescence measurements were done at room temperature. Concentration of solutions used in all the system was approximately up to 10^{-6} mol dm^{-3}. The lower the florescence intensity more is the binding with CD's, moreover it is found that in the α-CD inclusion with ALP the controlled release of the drug is more prominent ((Figure 9 (a), (b), (c)).[28]

8.3.4. XRD (or PXRD – powdered x-ray diffraction spectroscopy)

X-ray diffraction (XRD analysis or XRPD analysis) is an exclusive method in determination of crystallinity of a compound. It is primarily used for crystalline material of different polymorphic forms. Distinguishing among amorphous and crystalline material, quantification of the percent crystallinity of a sample is the mandatory criteria. We find (Figures.(10a, 10b, 10c,10d) the crystallinity changes in the complexes by definite angles.[28]

8.3.4. ESI-MS

The 'ESI-mass spectrometric analysis' were additionally used to recognize the formation of IC synthesized by procedure described above in the solid state of experimental procedure and have been shown in (Figure. 11(a), (b), (c)). Observation of peaks have been put, which verifies that in each cases the desired IC's have been formed in solid state and stoichiometric ratio of (host: guest) is (1:

1). The 'Positive electrospray ionization mass spectrometry' [ESI-MS] is enormously important process that has been used to examine host guest complexation with the two studied cyclodextrins. Mass spectrums of (1:1) stoichiometries of [α-CD: {ALP}], [β : {ALP} and [HP-β-CD: {ALP}] systems are evaluated by [ESI-MS] represents every preferred mass that one can expect. These experimental facts of the chosen [[ALP]/α-CD], [[ALP]/β-CD] and [[ALP] / HP-β-CD] complexes recommended that the [[ALP] + cation] simultaneously inserted in cyclodextrin's hollow space with (1:1) stoichiometry. [29]

8.3.4. Biological activity

ALP itself is non-toxic to cut micro flora. No zone of inhibition, in case of both the gram positive and gram negative organisms. There was no growth inhibition compared to control. These results recommend that ICs (IC1 = [ALP + α – CD], IC2 = [ALP + β-CD], IC3 = [ALP + HP-β-CD] doesn't have any antimicrobial activity shown in Figure 12 (a), (b), (c). So it is nontoxic for the cells experiment based on the sensitivity towards cut micro flora. There is no effect on cut-microbes- host interaction.[28].

Conclusion

Allopuinol sketch host-guest inclusion complexes together with (α-, β-, HP-β-) CD win the (1:1) stoichiometry which is recognized by UV, NMR, Steady state Fluorescence, SEM, HRMS imply that the selected guest (ALP) molecule, shaped IC's with nano hydrophobic core of efficiency. As a result the present work adjoins a new dimension in the diversified field of existing science of controlled release of allopurinol through appropriate host molecules like (α-, β-, HP-β-) CD.

4.5. REFERENCES

References of CHAPTER VI are given in BIBLIOGRAPHY (Page No.300-302)

Tables

Table 1.Data of Job's plot between ALP and α-CD obtained from UV spectroscopy

ALP(ml)	α-CD(ml)	ALP(μM)	α-CD(μM)	[ALP]/ ([ALP]+[αCD])	ABSORBANCE	ΔA	ΔA*[ALP]/ ([ALP]+[αCD])
4	0	100	0	1	3.543	0	0
3.6	0.4	90	10	0.9	3.743	0.2	0.18
3.2	0.8	80	20	0.8	3.416	0.327	0.2616
2.8	1.2	70	30	0.7	3.416	0	0
2.4	1.6	60	40	0.6	2.909	0.507	0.3042
2	2	50	50	0.5	2.563	0.346	0.173
1.6	2.4	40	60	0.4	2.133	0.43	0.172
1.2	2.8	30	70	0.3	1.783	0.35	0.105
0.8	3.2	20	80	0.2	1.272	0.511	0.1022
0.4	3.6	10	90	0.1	0.877	0.395	0.0395
0	4	0	100	0	0.299	0.578	0

Table 2. Data of Job's plot between ALP and β-CD obtained from UV spectroscopy

ALP(ml)	β-CD(ml)	ALP(μM)	β-CD(μM)	[ALP]/([ALP]+[βCD])	ABSORBANCE	ΔA	ΔA*[ALP]/([ALP]+[β-CD])
4	0	100	0	1	3.997	0.324	1.345
3.6	0.4	90	10	0.9	3.998	0.456	1.461
3.2	0.8	80	20	0.8	3.999	0.567	1.562
2.8	1.2	70	30	0.7	3.999	0.782	1.721
2.4	1.6	60	40	0.6	3.096	0.903	2.503
2	2	50	50	0.5	2.588	0.508	2.508
1.6	2.4	40	60	0.4	2.302	0.286	2.686
1.2	2.8	30	70	0.3	1.73	0.572	3.372
0.8	3.2	20	80	0.2	0.821	0.909	4.109
0.4	3.6	10	90	0.1	0.778	0.043	3.643
0	4	0	100	0	0.417	0.361	3.175

Table 3. Data of Job's plot between ALP and HP-β-CD obtained from UV spectroscopy

ALP (ml)	HP-β-CD (ml)	ALP (μM)	HP-β-CD (μM)	[ALP]/ ([ALP]+[HP-β-CD])	ABSORBANCE	ΔA	ΔA*[ALP]/ ([ALP]+[β-CD])
4	0	100	0	1	3.573	0	0
3.6	0.4	90	10	0.9	3.959	0.386	10.386
3.2	0.8	80	20	0.8	3.965	0.006	20.006
2.8	1.2	70	30	0.7	3.999	0.034	30.034
2.4	1.6	60	40	0.6	3.337	0.662	39.338
2	2	50	50	0.5	1.844	1.493	48.507

1.6	2.4	40	60	0.4	1.435	0.409	59.591
1.2	2.8	30	70	0.3	1.225	0.21	69.79
0.8	3.2	20	80	0.2	0.959	0.266	79.734
0.4	3.6	10	90	0.1	0.751	0.208	89.792
0	4	0	100	0	0.58	0.171	0

Table 4. Data for the Benesi-Hildebrand double reciprocal plot performed by UV-VIS spectroscopic study for [ALP]-α-CD systems at (293.15, 298.15, and 303.15) K

temp/k	[ALP]/µM	[α-CD]/µM	A_o	A	ΔA	1/[α-CD]/M−1	1/ΔA
	50	30	0.9926	1.1745	0.1819	0.033333333	5.497526
	50	40	0.9926	1.1913	0.1987	0.025	5.032713
293.15K	50	50	0.9926	1.2028	0.2102	0.02	4.757374
	50	60	0.9926	1.2239	0.2313	0.016666667	4.32339
	50	70	0.9926	1.2484	0.2558	0.014285714	3.909304
	50	80	0.9926	1.2684	0.2758	0.0125	3.625816
	50	90	0.9926	1.2747	0.2821	0.011111111	3.544842
298.15K	50	30	0.9926	1.2789	0.2863	0.033333333	3.49284
	50	40	0.9926	1.2986	0.306	0.025	3.267974
	50	50	0.9926	1.3535	0.3609	0.02	2.770851
	50	60	0.9926	1.3867	0.3941	0.016666667	2.537427
	50	70	0.9926	1.4269	0.4343	0.014285714	2.302556
	50	80	0.9926	1.5034	0.5108	0.0125	1.957713
	50	90	0.9926	1.5594	0.5668	0.011111111	1.764291
303.15K	50	30	0.9926	1.5096	0.517	0.033333333	1.934236
	50	40	0.9926	1.5791	0.5865	0.025	1.70503
	50	50	0.9926	1.62991	0.63731	0.02	1.569095
	50	60	0.9926	1.6715	0.6789	0.016666667	1.472971
	50	70	0.9926	1.7286	0.736	0.014285714	1.358696
	50	80	0.9926	1.8247	0.8321	0.0125	1.201779
	50	90	0.9926	1.9105	0.9179	0.011111111	1.089443

Table 5. Data for the Benesi-Hildebrand double reciprocal plot performed by UV-VIS spectroscopic study for [ALP]-β-CD systems at (293.15, 298.15, and 303.15) K

temp/k	[ALP]/µM	[β-CD]/µM	A_o	A	ΔA	1/[β-CD]/M−1	1/ΔA
	50	30	0.9926	1.2854	0.2928	0.033333333	3.415301
	50	40	0.9926	1.3185	0.3259	0.025	3.068426
293.15K	50	50	0.9926	1.3883	0.3957	0.02	2.527167
	50	60	0.9926	1.4331	0.4405	0.016666667	2.270148
	50	70	0.9926	1.5281	0.5355	0.014285714	1.867414
	50	80	0.9926	1.6621	0.6695	0.0125	1.493652
	50	90	0.9926	1.7315	0.7389	0.011111111	1.353363
298.15K	50	30	0.9926	1.1892	0.1966	0.033333333	5.08647

	50	40	0.9926	1.2538	0.2612	0.025	3.828484
	50	50	0.9926	1.2706	0.278	0.02	3.597122
	50	60	0.9926	1.3555	0.3629	0.016666667	2.75558
	50	70	0.9926	1.4366	0.444	0.014285714	2.252252
	50	80	0.9926	1.5434	0.5508	0.0125	1.815541
	50	90	0.9926	1.628	0.6354	0.011111111	1.573812
303.15K	50	30	0.9926	1.386	0.3934	0.033333333	2.541942
	50	40	0.9926	1.4405	0.4479	0.025	2.232641
	50	50	0.9926	1.3297	0.3371	0.02	2.966479
	50	60	0.9926	1.5344	0.5418	0.016666667	1.8457
	50	70	0.9926	2.0923	1.0997	0.014285714	0.909339
	50	80	0.9926	2.1743	1.1817	0.0125	0.846238
	50	90	0.9926	2.3721	1.3795	0.011111111	0.7249

Table 6. Data for the Benesi-Hildebrand double reciprocal plot performed by UV-VIS spectroscopic study for [ALP]-HP-β-CD systems at (293.15, 298.15, and 303.15) K

temp/k	[ALP]/μM	[HP-β-CD]/μM	$A_{\circ}$	A	ΔA	1/[HP-β-CD]/M−1	1/ΔA
	50	30	0.9926	1.3111	0.3185	0.033333333	3.139717
	50	40	0.9926	1.3448	0.3522	0.025	2.839296
293.15K	50	50	0.9926	1.3612	0.3686	0.02	2.712968
	50	60	0.9926	1.4141	0.4215	0.016666667	2.372479
	50	70	0.9926	1.4519	0.4593	0.014285714	2.177226
	50	80	0.9926	1.5249	0.5323	0.0125	1.87864
	50	90	0.9926	1.5283	0.5357	0.011111111	1.866716
298.15K	50	30	0.9926	1.1863	0.1937	0.033333333	5.162623
	50	40	0.9926	1.2217	0.2291	0.025	4.364906
	50	50	0.9926	1.2501	0.2575	0.02	3.883495
	50	60	0.9926	1.3222	0.3296	0.016666667	3.033981
	50	70	0.9926	1.4299	0.4373	0.014285714	2.28676
	50	80	0.9926	1.5463	0.5537	0.0125	1.806032
	50	90	0.9926	1.6234	0.6308	0.011111111	1.585289
303.15K	50	30	0.9926	1.3078	0.3152	0.033333333	3.172589
	50	40	0.9926	1.4467	0.4541	0.025	2.202158
	50	50	0.9926	1.5219	0.5293	0.02	1.889288
	50	60	0.9926	1.6324	0.6398	0.016666667	1.562988
	50	70	0.9926	1.7565	0.7639	0.014285714	1.309072
	50	80	0.9926	1.8435	0.8509	0.0125	1.175226
	50	90	0.9926	1.91	0.9174	0.011111111	1.090037

FIGURES

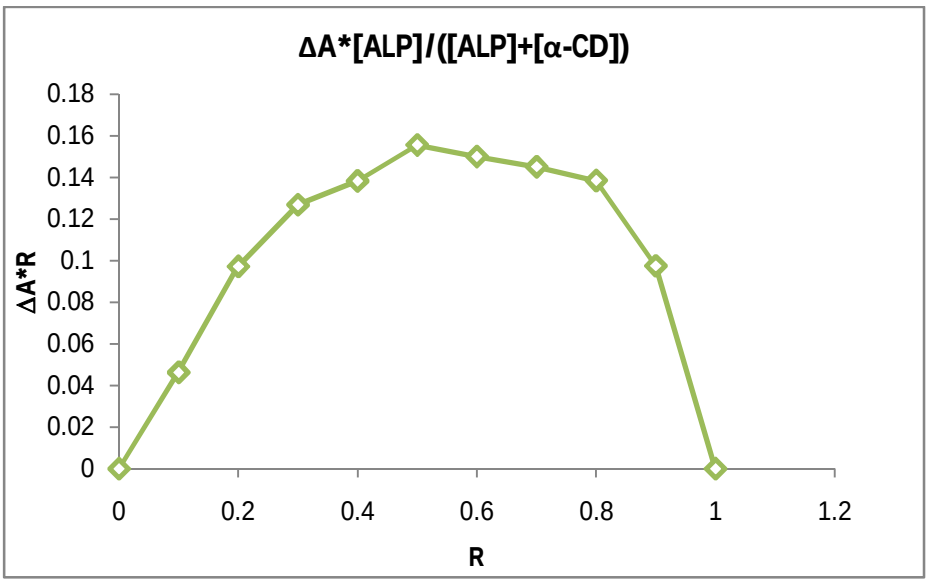

Figure 1a. Job's Plot for [ALP] with α-CD

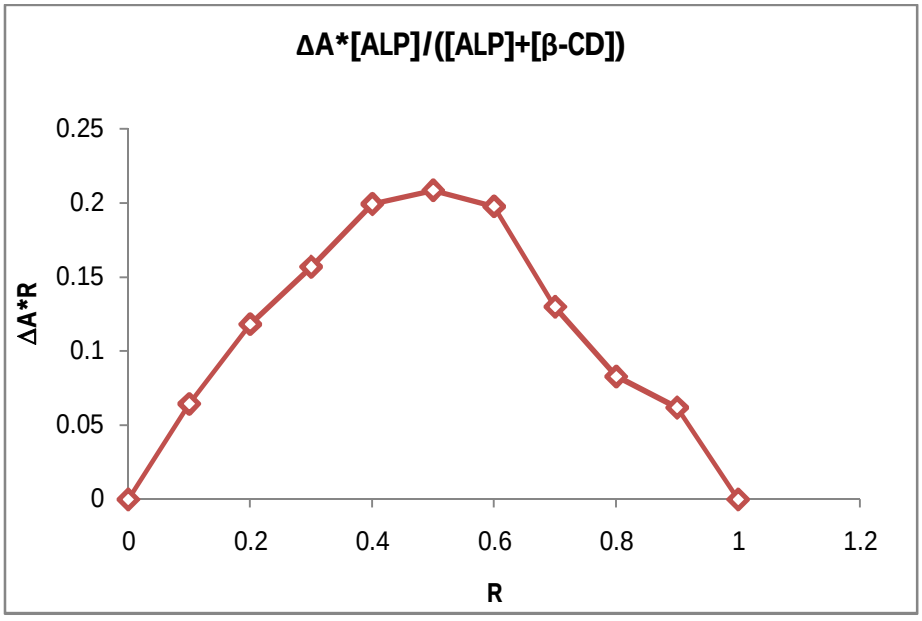

Figure 1b. Job's Plot for [ALP] with β-CD

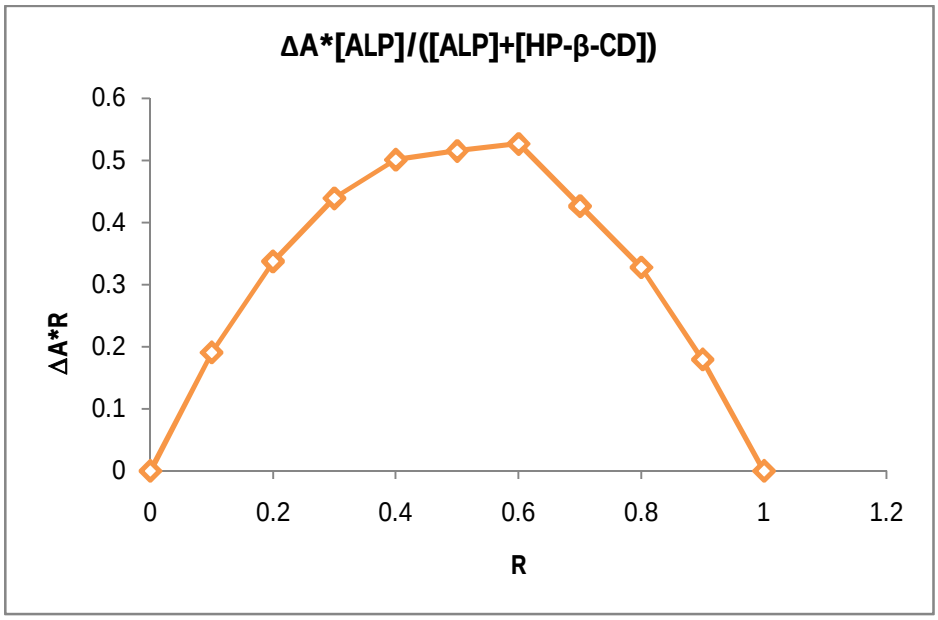

Figure 1c. Job's Plot for [ALP] with HP-β-CD

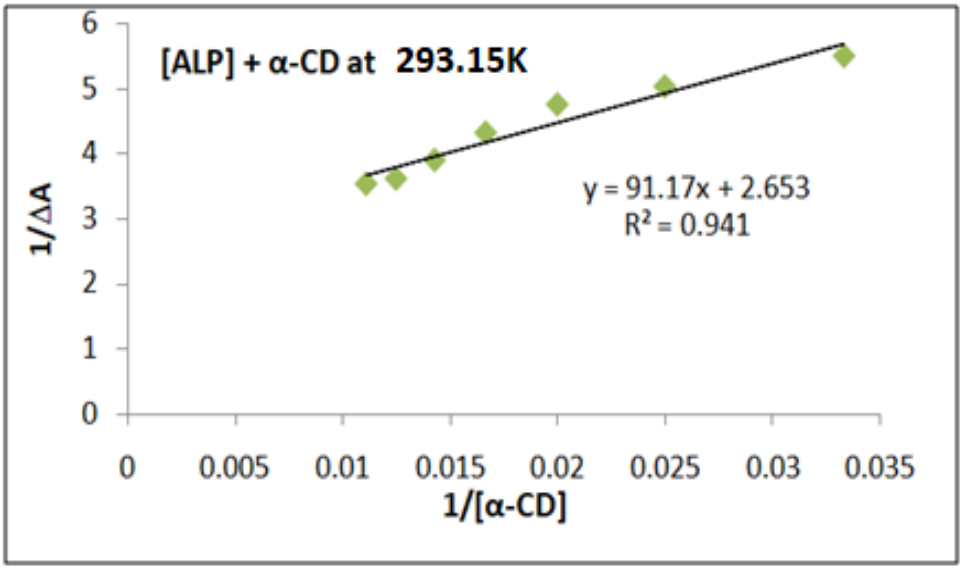

Figure 2a. Benesi-Hildebrand double reciprocal plots for the effect of α-CD on the absorbance of [ALP] at 293.15K

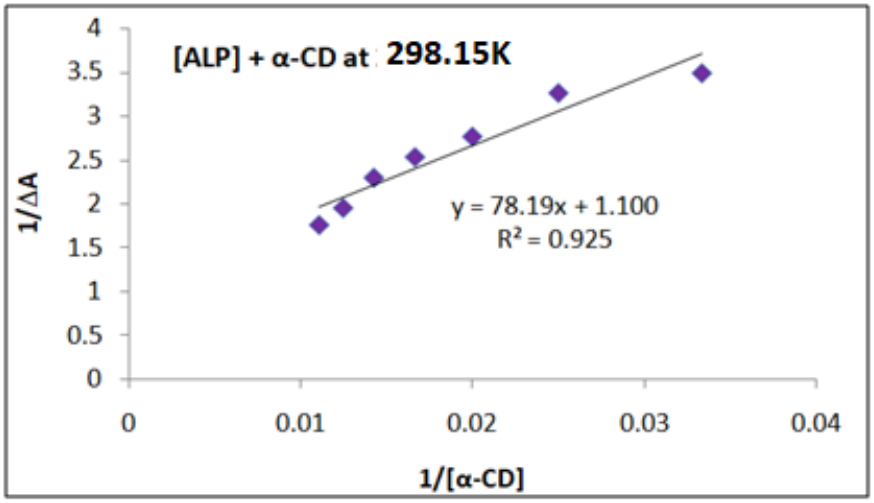

Figure 2b. Benesi-Hildebrand double reciprocal plots for the effect of α-CD on the absorbance of [ALP] at 298.15K

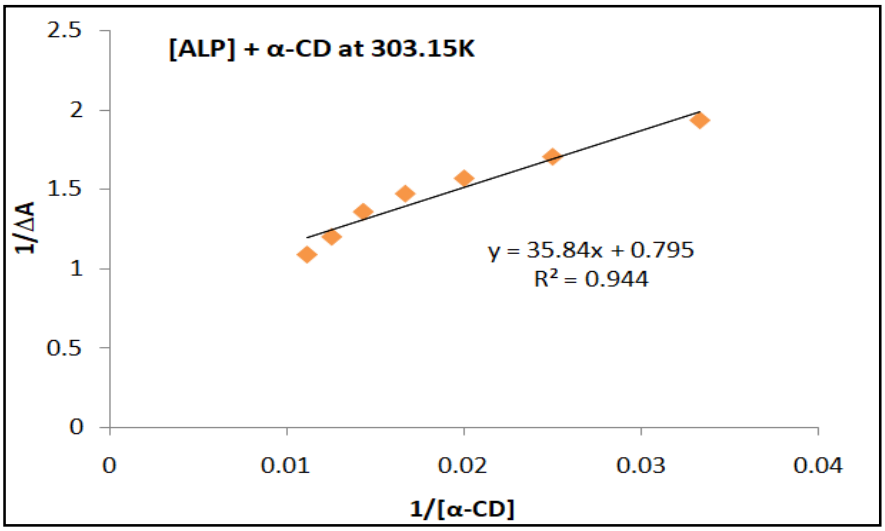

Figure 2c. Benesi-Hildebrand double reciprocal plots for the effect of α-CD on the absorbance of [ALP] at 303.15K

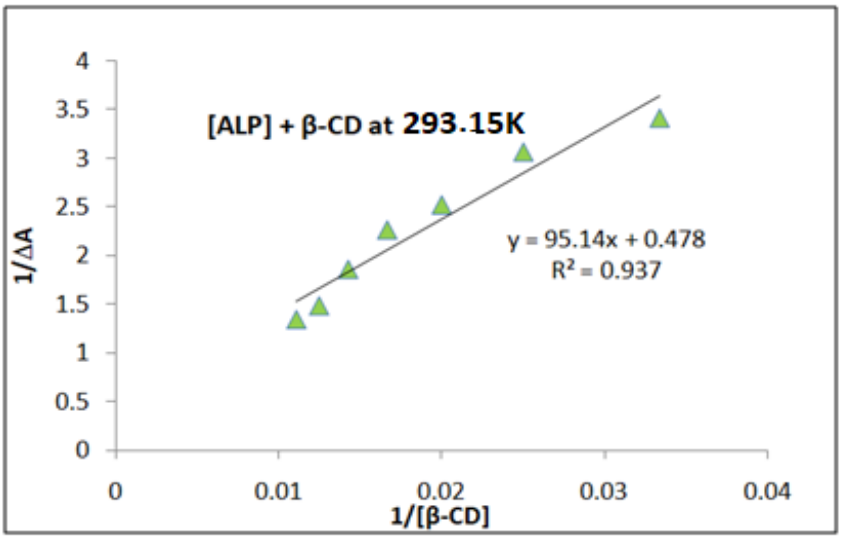

Figure 3a. Benesi-Hildebrand double reciprocal plots for the effect of β-CD on the absorbance of [ALP] at 293.15K

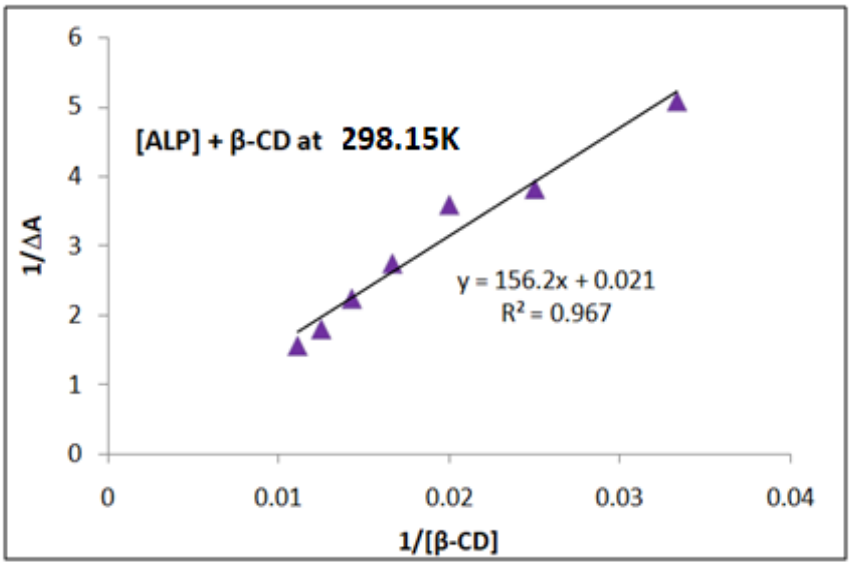

Figure 3b. Benesi-Hildebrand double reciprocal plots for the effect of β-CD on the absorbance of [ALP] at 298.15K

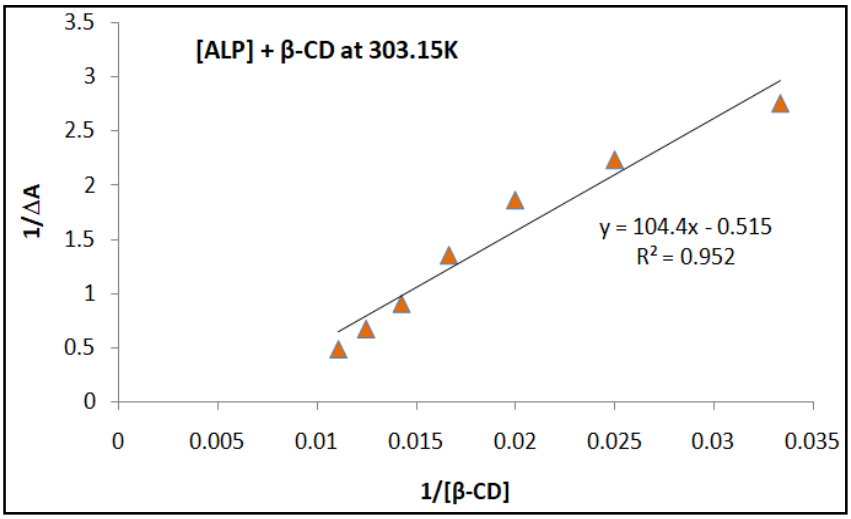

Figure 3c. Benesi-Hildebrand double reciprocal plots for the effect of β-CD on the absorbance of [ALP] at 303.15K

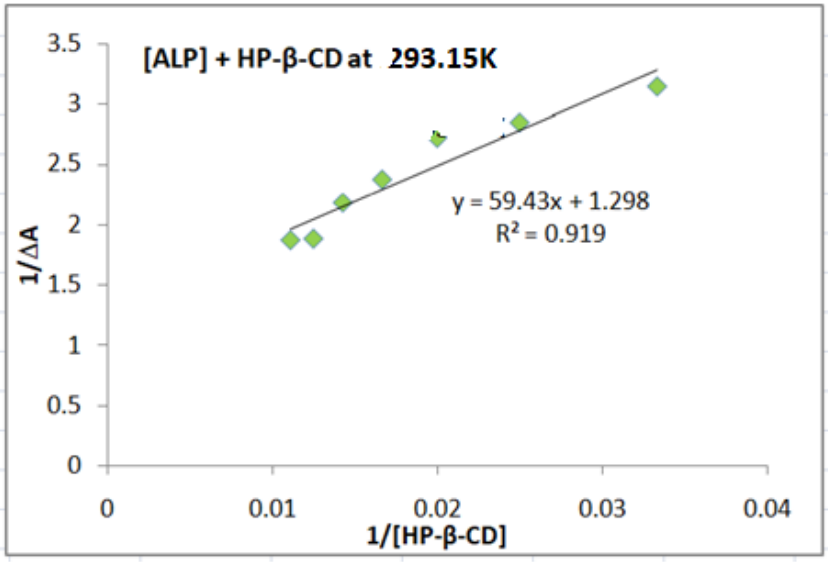

Figure 4a. Benesi-Hildebrand double reciprocal plots for the effect of HP-β-CD on the absorbance of [ALP] at 293.15K

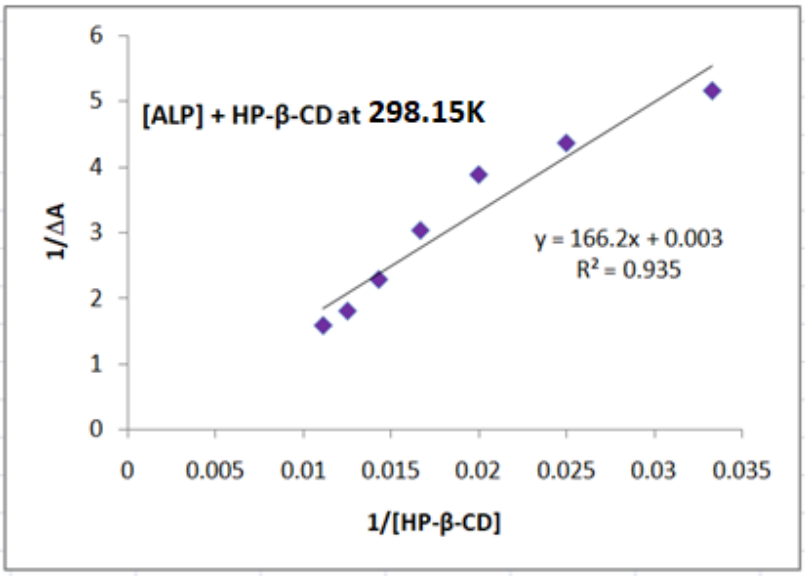

Figure 4b. Benesi-Hildebrand double reciprocal plots for the effect of HP-β-CD on the absorbance of [ALP] at 298.15K

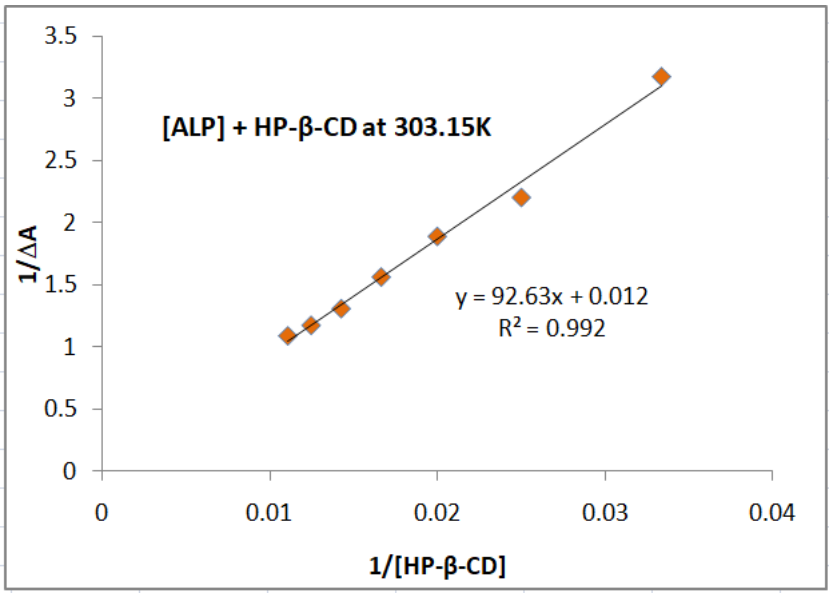

Figure 4c. Benesi-Hildebrand double reciprocal plots for the effect of HP-β-CD on the absorbance of [ALP] at 303.15K

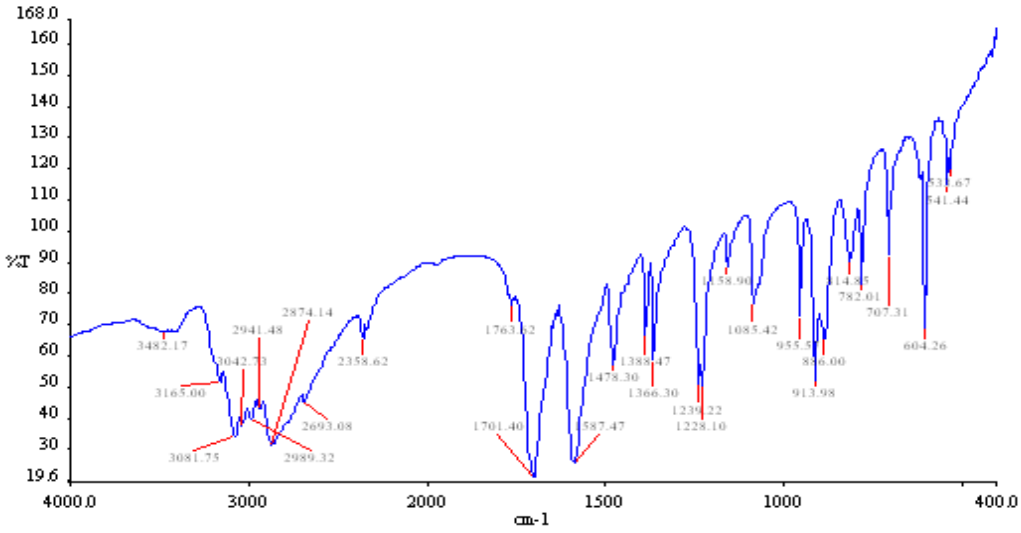

Figure .5(a): FT-IR spectra of (pure [ALP]) at 298.15K

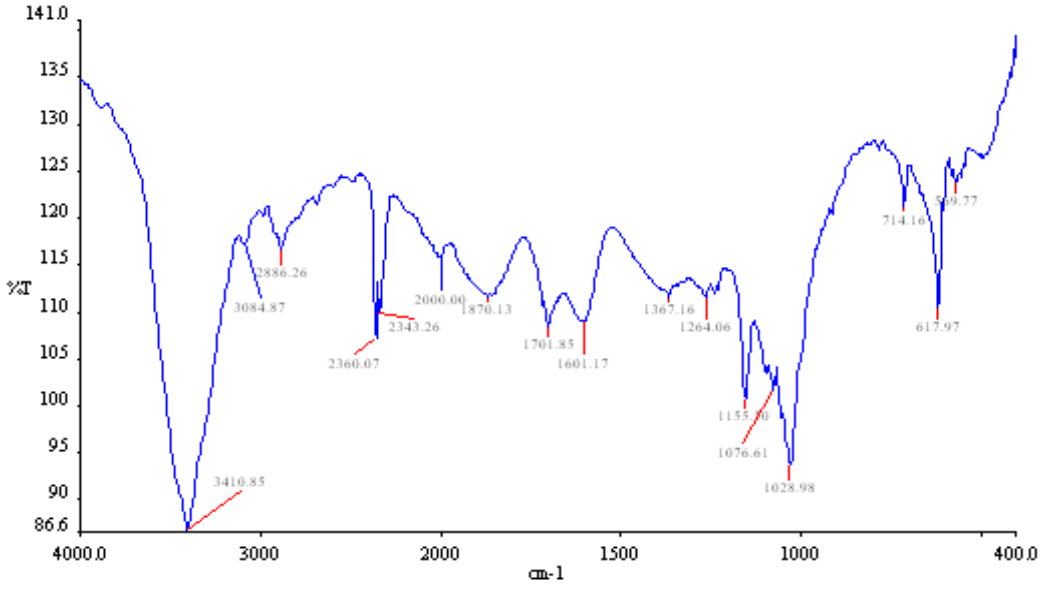

Figure.5(b): FT-IR spectra of 1:1 inclusion complexes ([ALP] + α-CD) at 298.15K

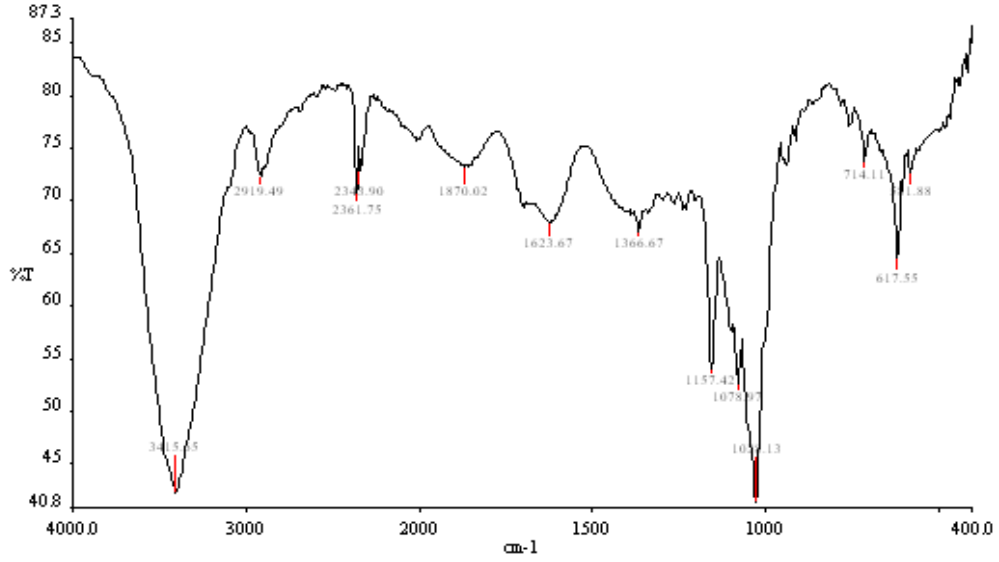

Figure .5(c): FT-IR spectra of 1:1 inclusion complexes ([ALP] + β-CD) at 298.15K

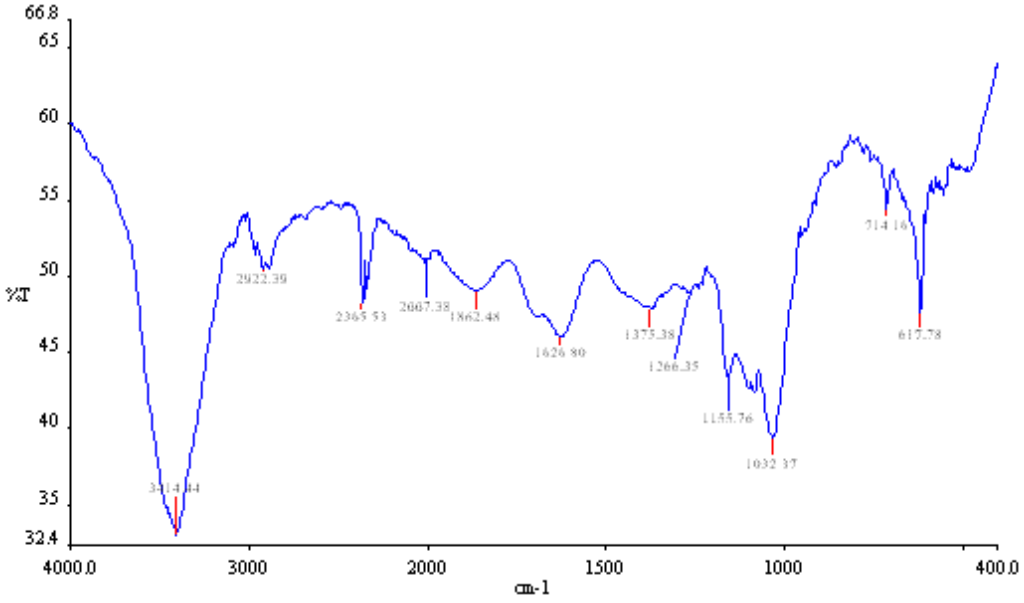

Figure .5(d): FT-IR spectra of 1:1 inclusion complexes ([ALP] + HP-β-CD) at 298.15K

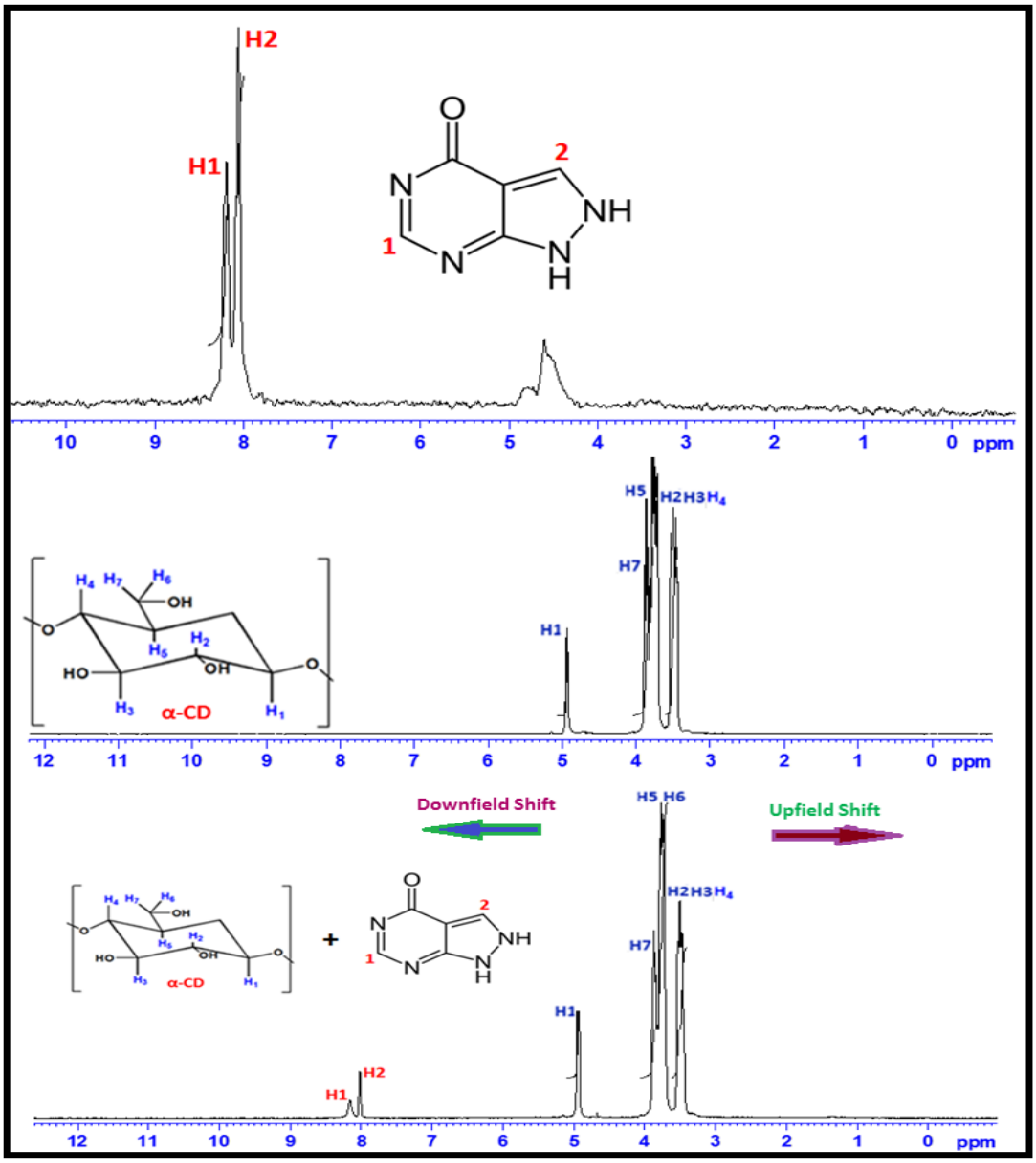

Figure 6(a). 1H-NMR spectra of the pure compounds and inclusion complexes with α-CD at 298.15K (400MHz, D_2O)

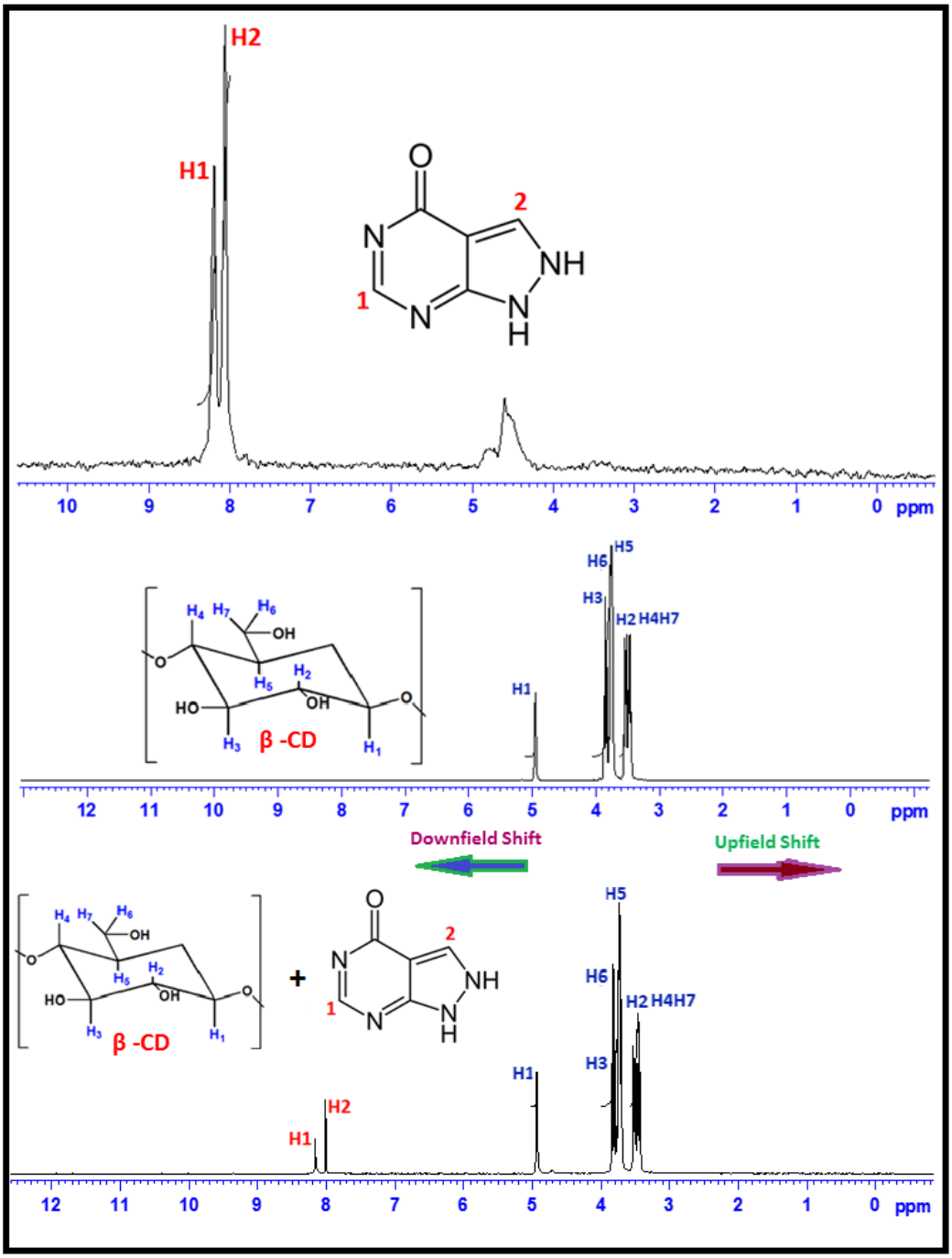

Figure 6(b). 1H-NMR spectra of the pure compounds and inclusion complexes with β-CD at 298.15K (400MHz, D_2O)

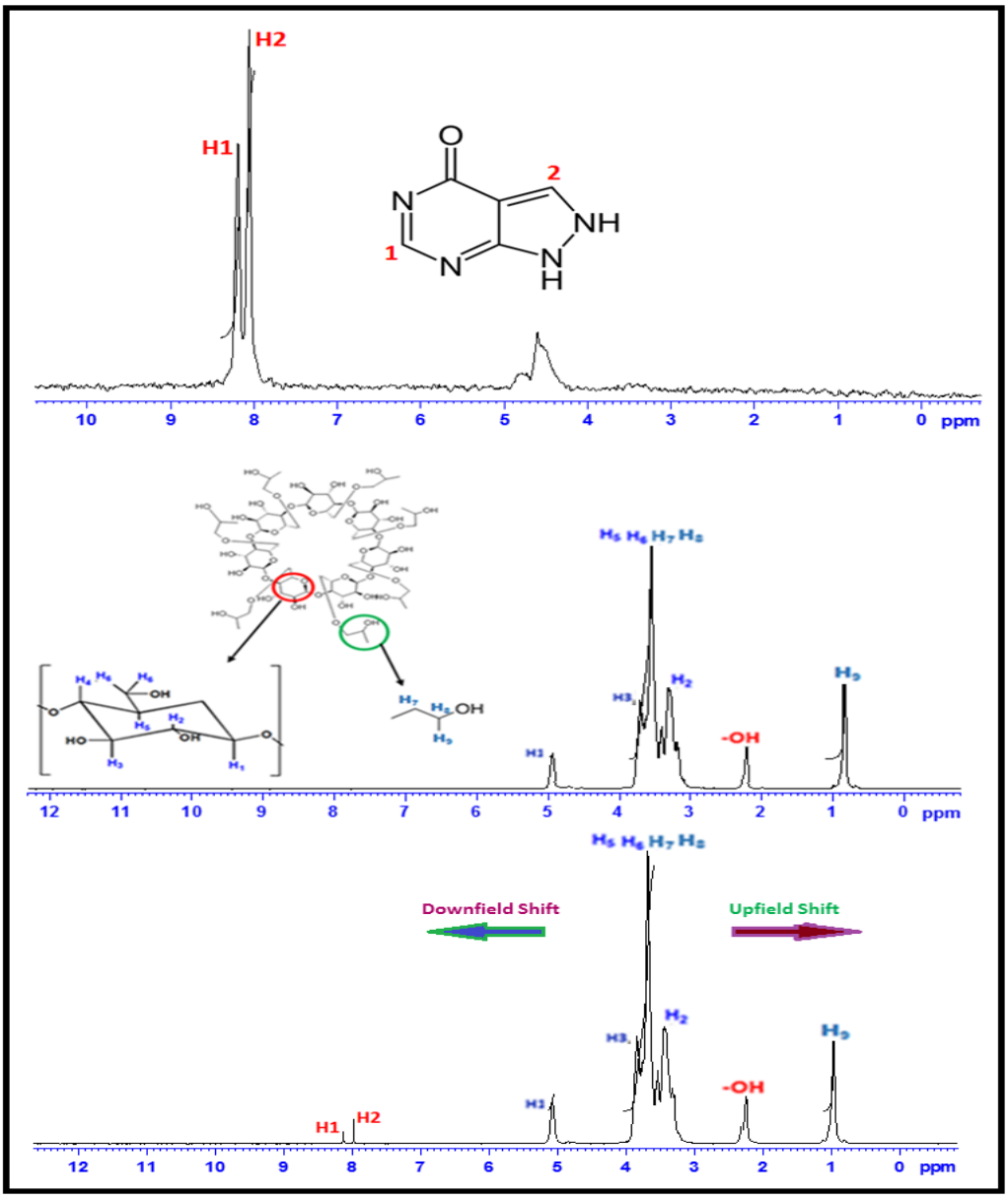

Figure 6(c). 1H-NMR spectra of the pure compounds and inclusion complexes with HP-β-CD at 298.15K (400MHz, D_2O)

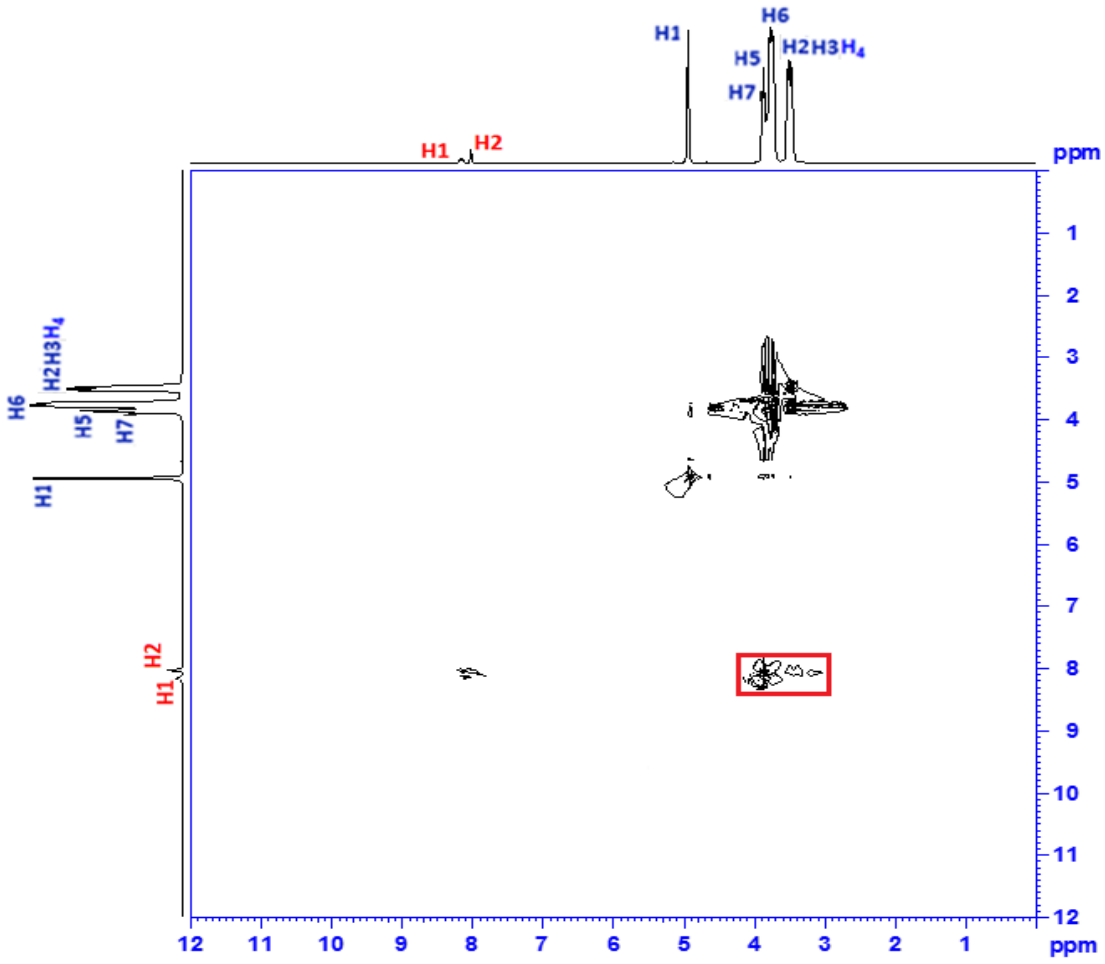

Figure 7(a). 2D ROESY spectra of the solid ICs of [ALP].α-CD in D2O. (Cross correlations are indicated by red circles)

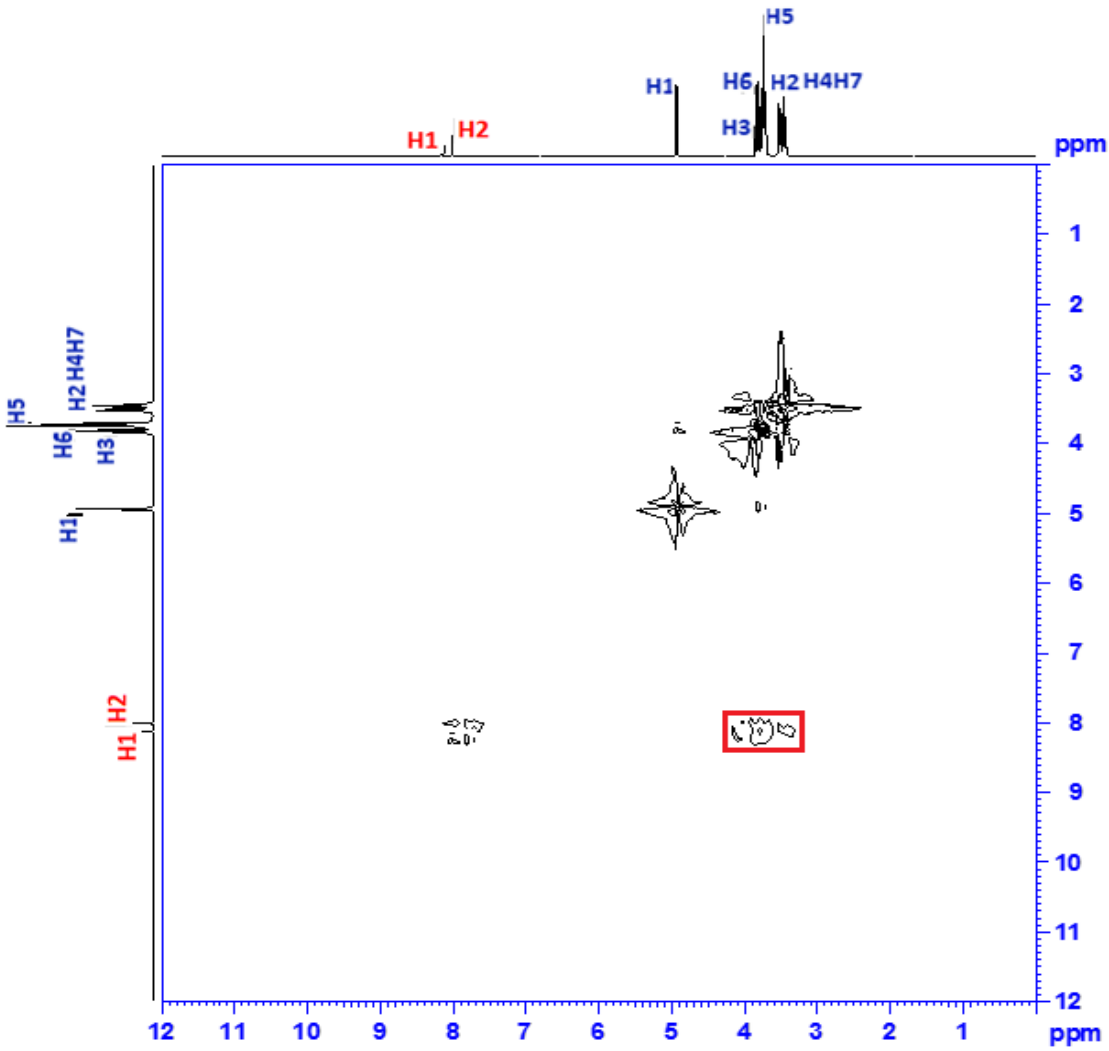

Figure 7(b). 2D ROESY spectra of the solid ICs of [ALP].β-CD in D2O. (Cross correlations are indicated by red circles)

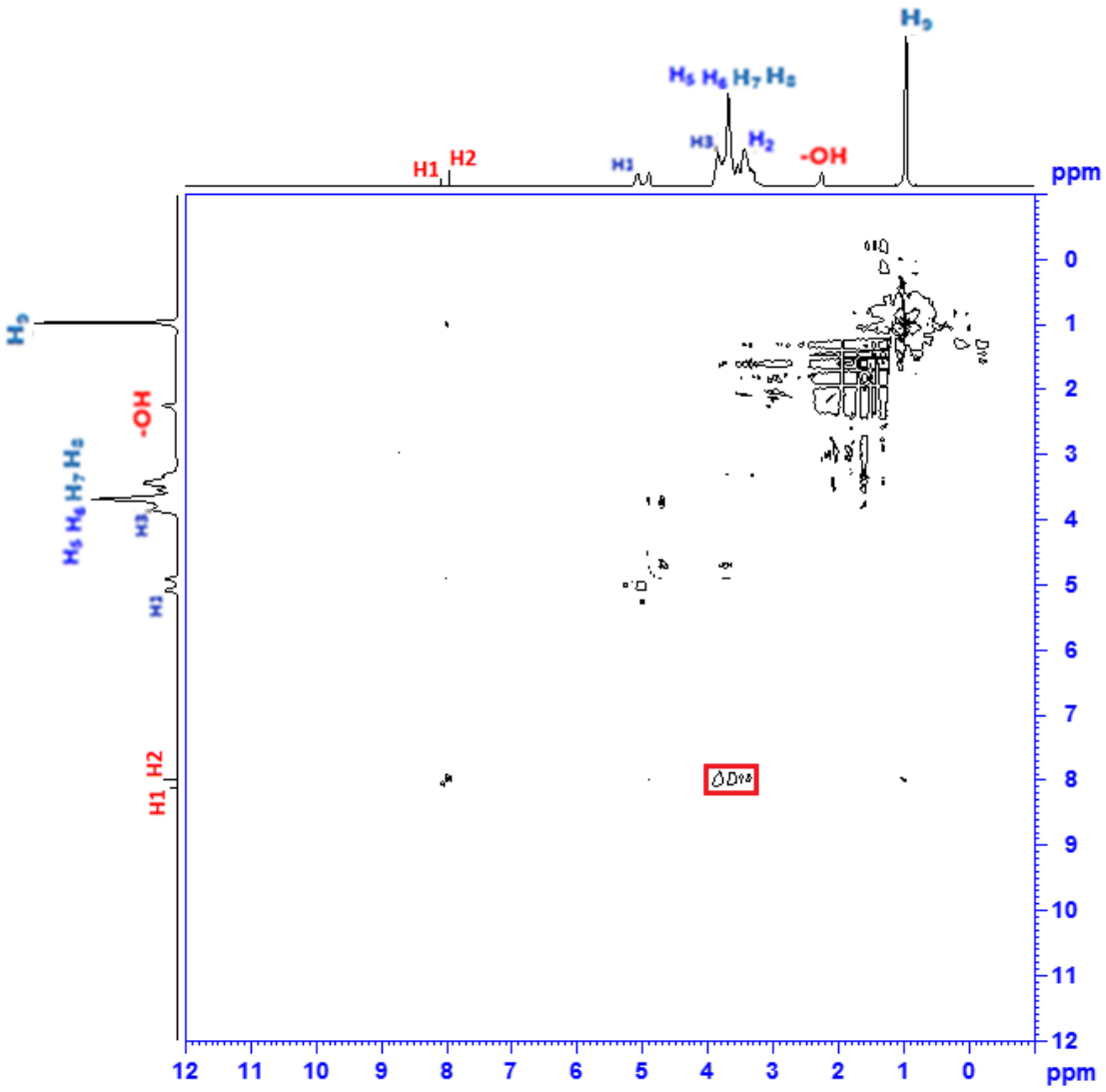

Figure7(c). 2D ROESY spectra of the solid ICs of [ALP].HP-β-CD in D2O. (Cross correlations are indicated by red circles)

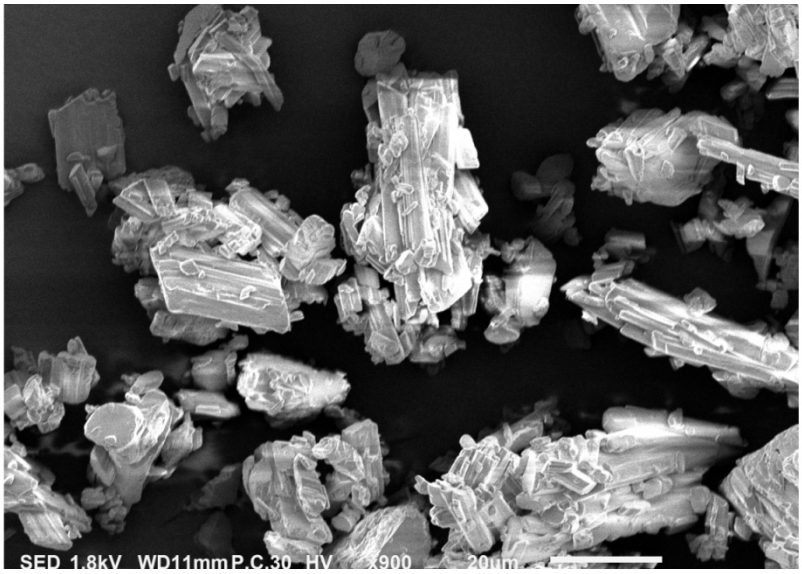

Figure 8(a). (SEM) showing morphologic study of ALP in (1:1 M ratio) of inclusion complex

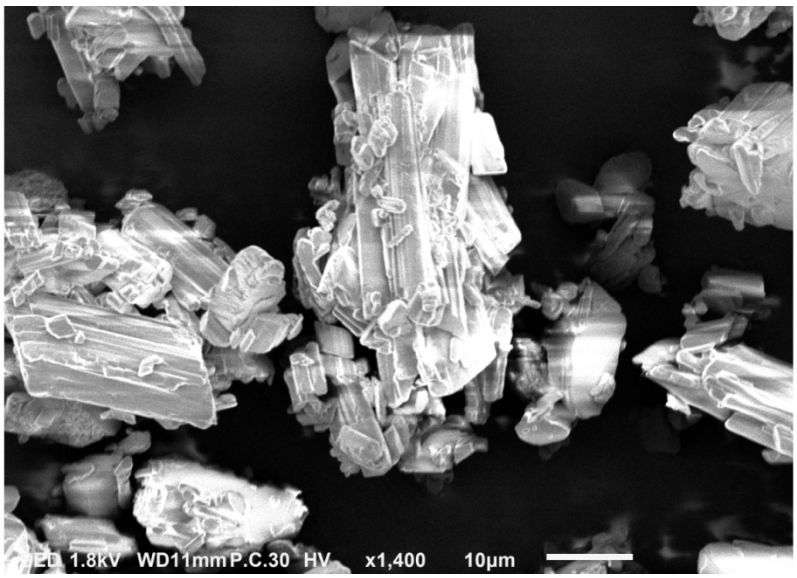

Figure 8(b). (SEM) showing morphologic study of [ALP: (α-CD)] in (1:1 M ratio) of inclusion complex

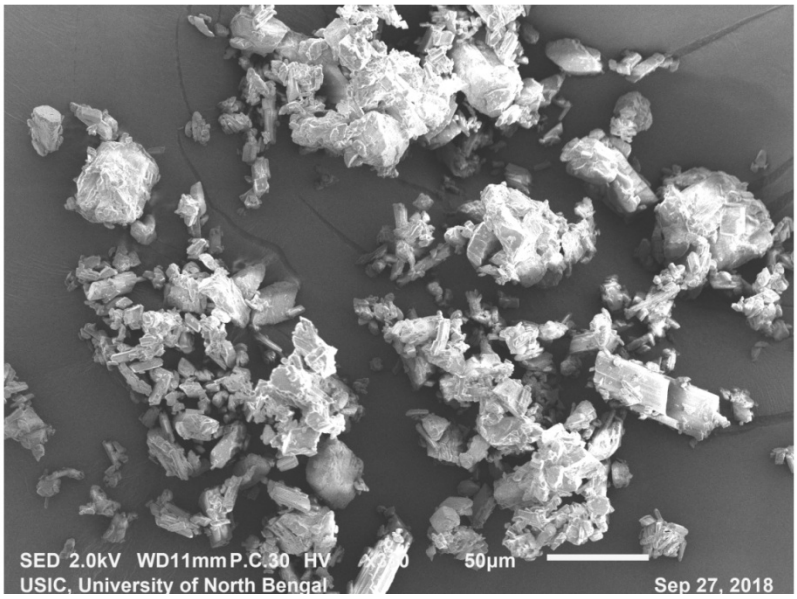

Figure 8(c). (SEM) showing morphologic study of [ALP: (β-CD)] in (1:1 M ratio) of inclusion complex

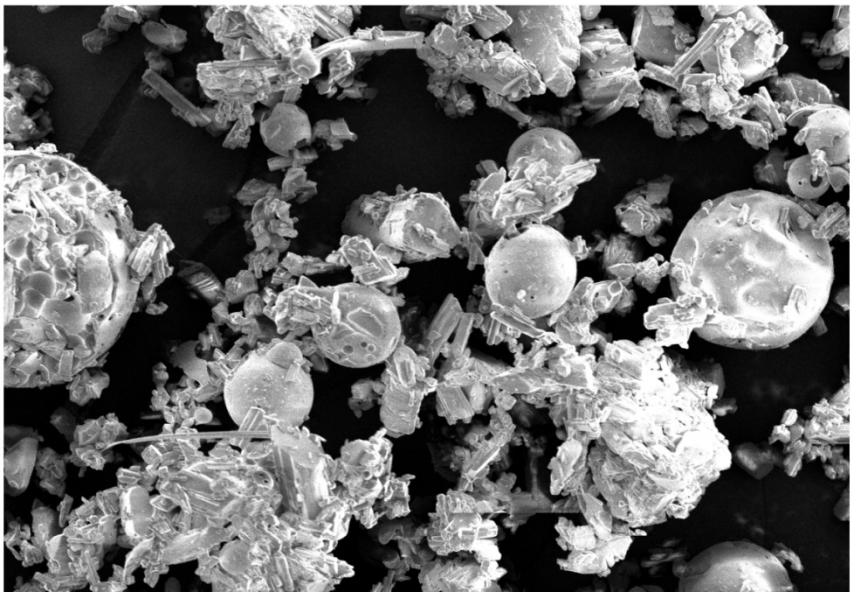

Figure 8(d). (SEM) showing morphologic study of [ALP: (HP-β-CD)] in (1:1 M ratio) of inclusion complex

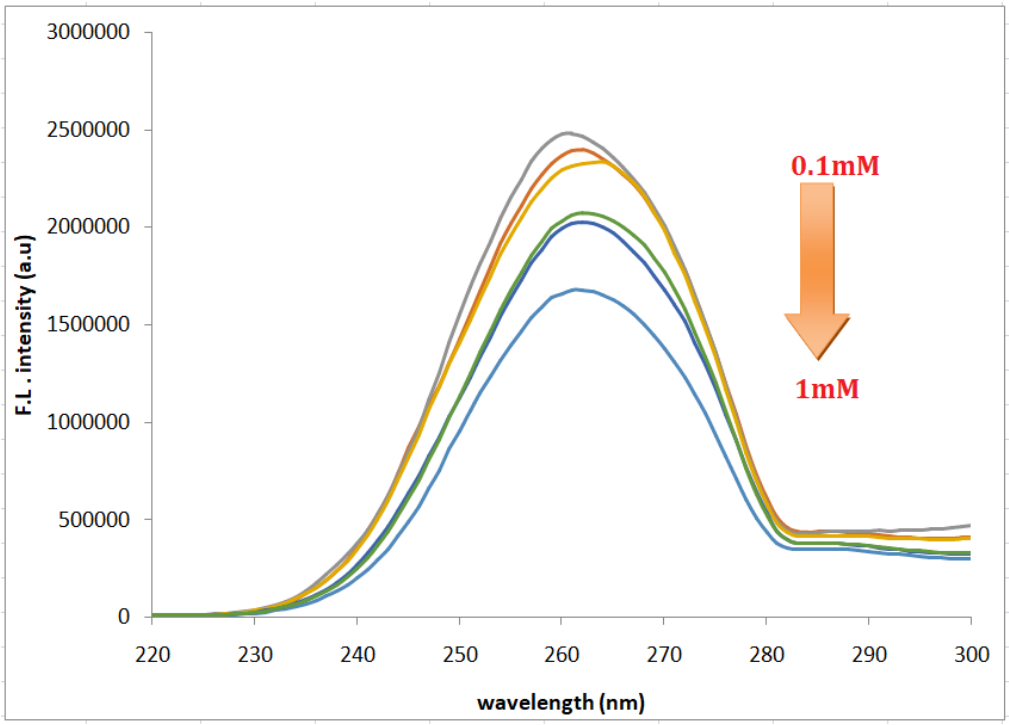

Figure 9(a). Fluorescence emission spectrum of aqueous (α-CD) in presence of (0.1mM–1.0 mM) of ALP (λ_{ex} =250 nm, slit width =5/5)

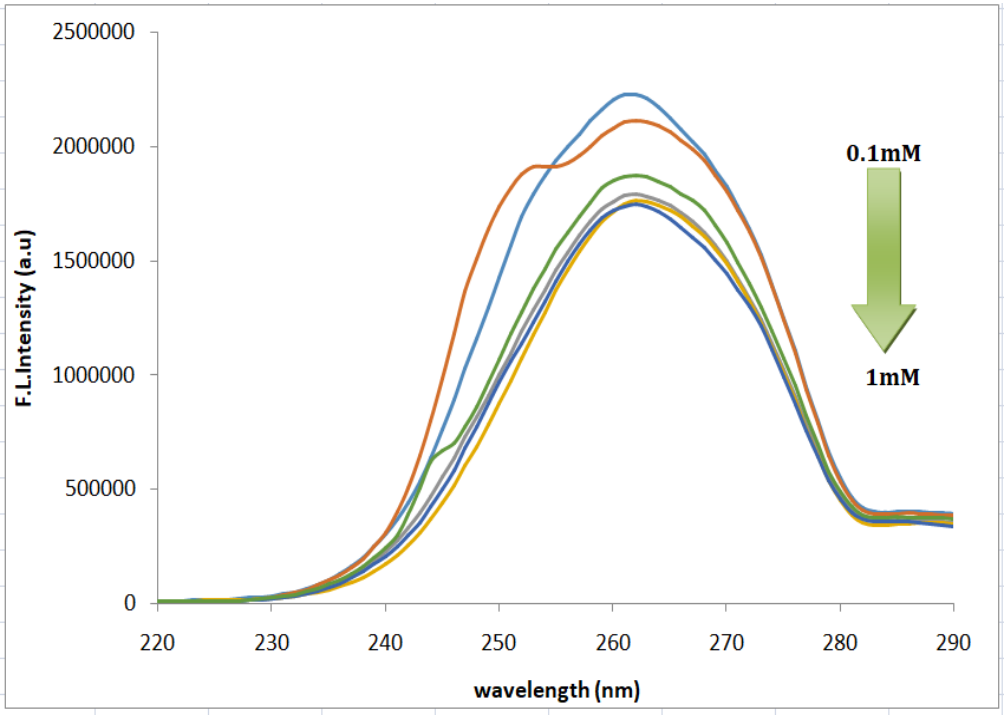

Figure 9(b). Fluorescence emission spectrum of aqueous (β-CD) in presence of (0.1mM–1.0 mM) of ALP (λ_{ex} =250 nm, slit width =5/5).

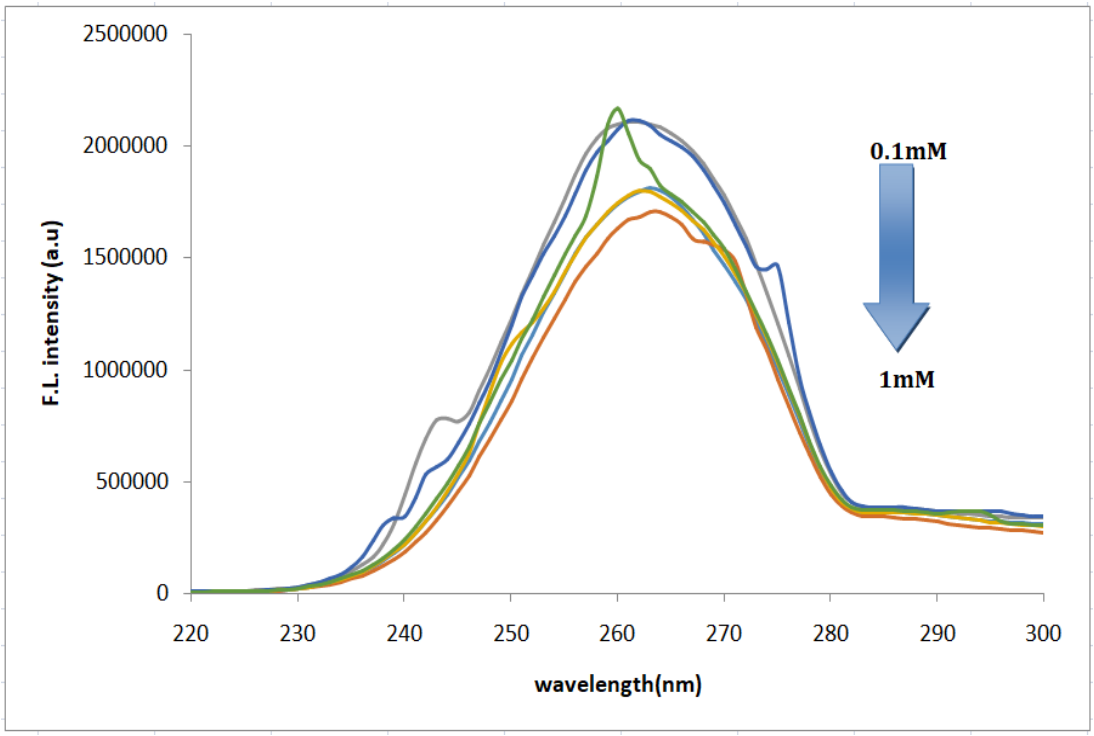

Figure 9(c). Fluorescence emission spectrum of aqueous (HP-β-CD) in presence of (0.1mM–1.0 mM) of ALP (λ_{ex} =250 nm, slit width =5/5).

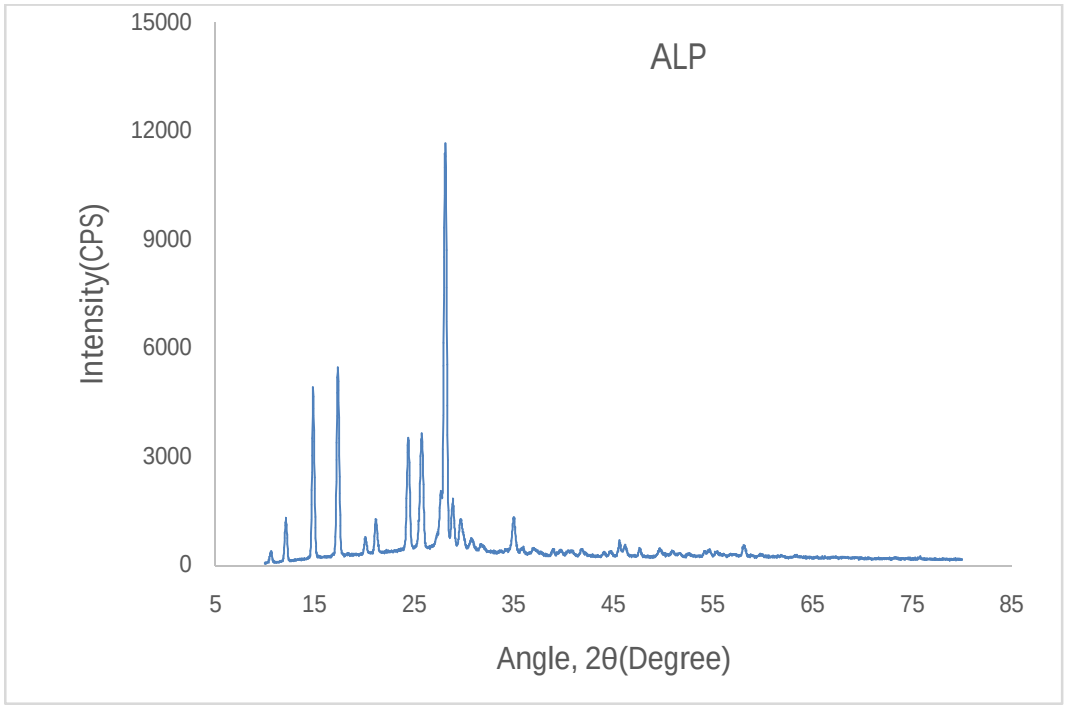

Figure10(a). Powder X-ray diffraction pattern of ALP

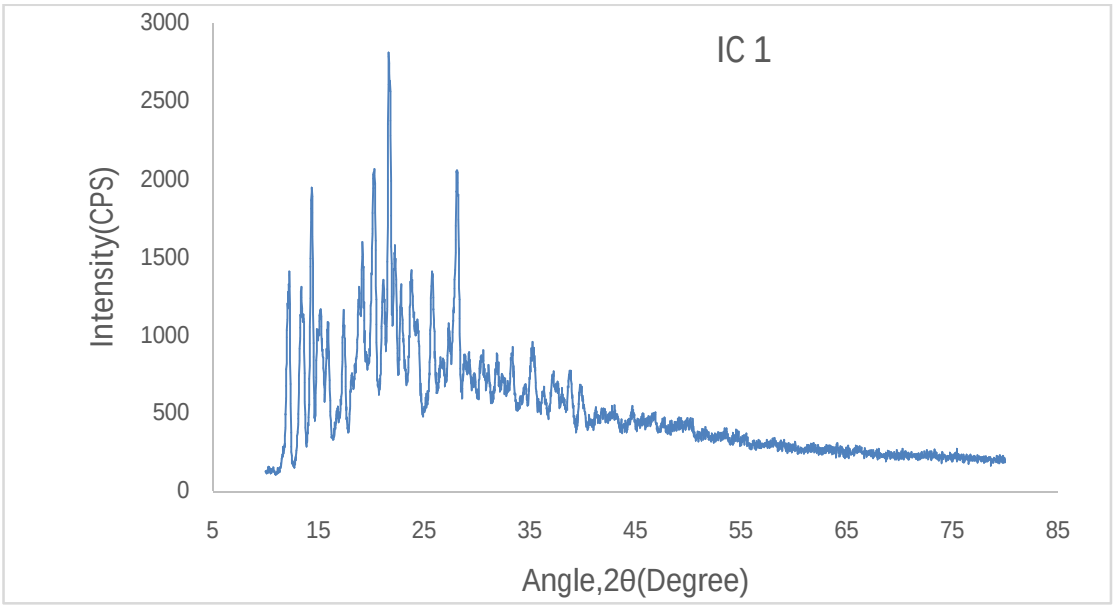

Figure10(b). Powder X-ray diffraction pattern of ALP+ α-CD

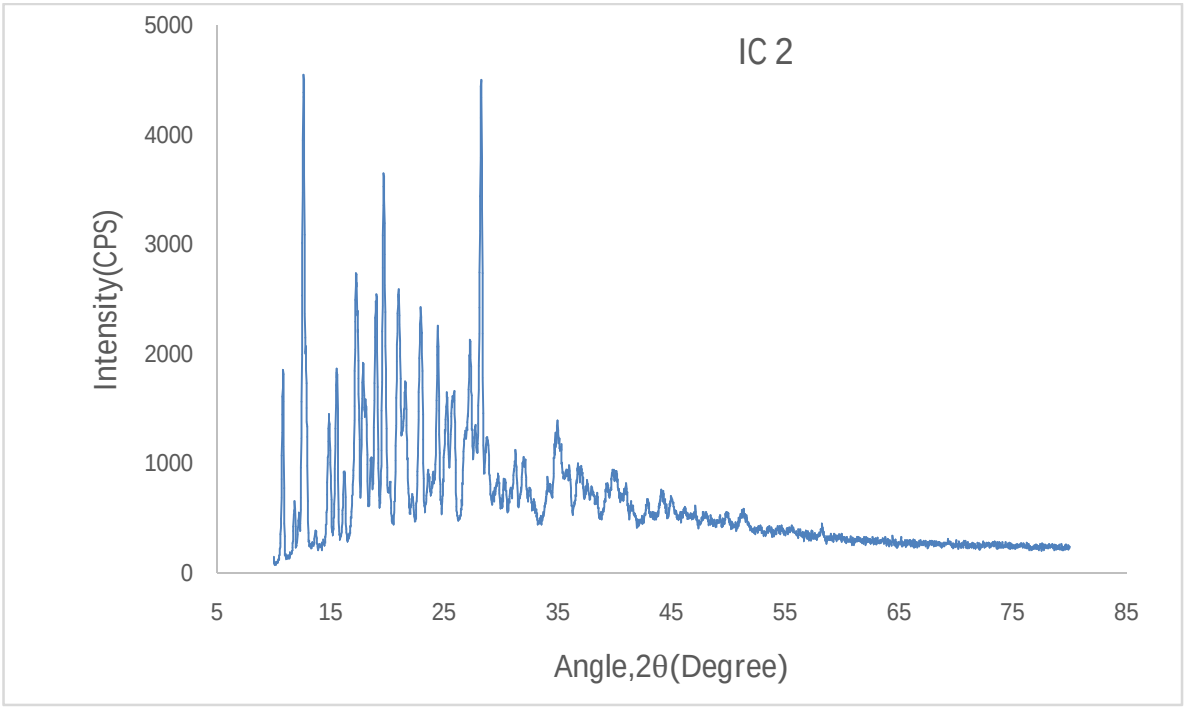

Figure10(c). Powder X-ray diffraction pattern of ALP+β-CD

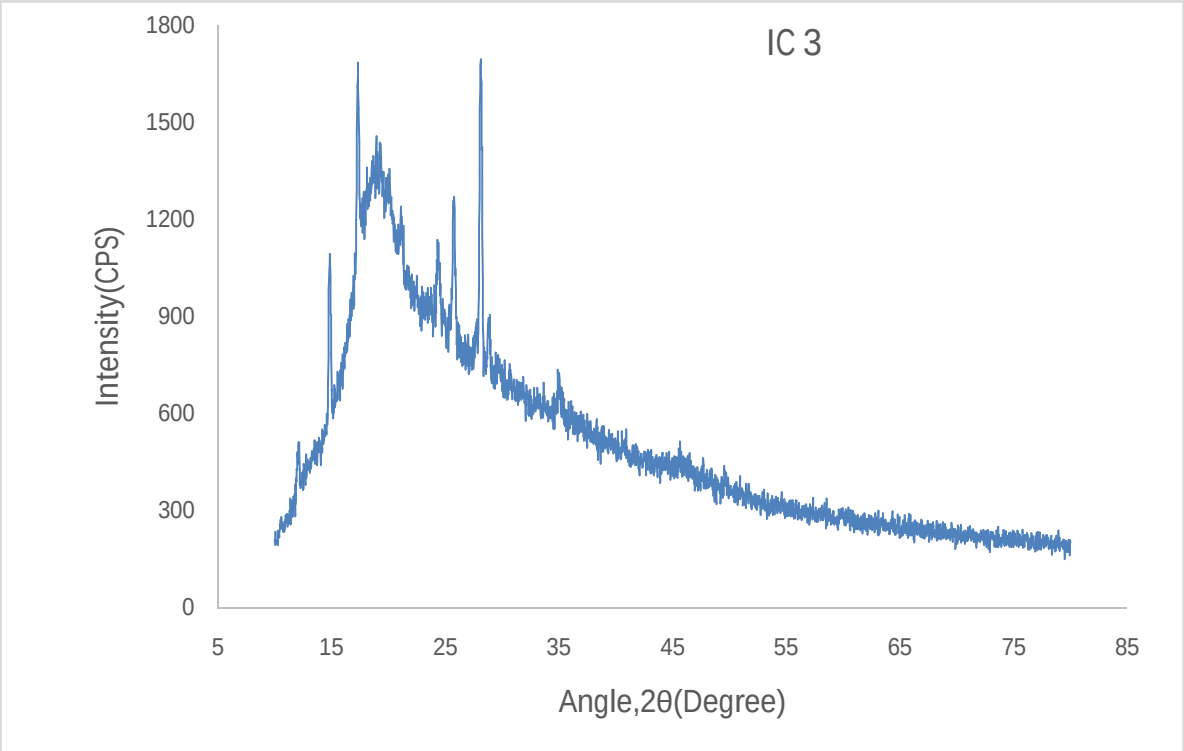

Figure10(d). Powder X-ray diffraction pattern of ALP+HP-β-CD

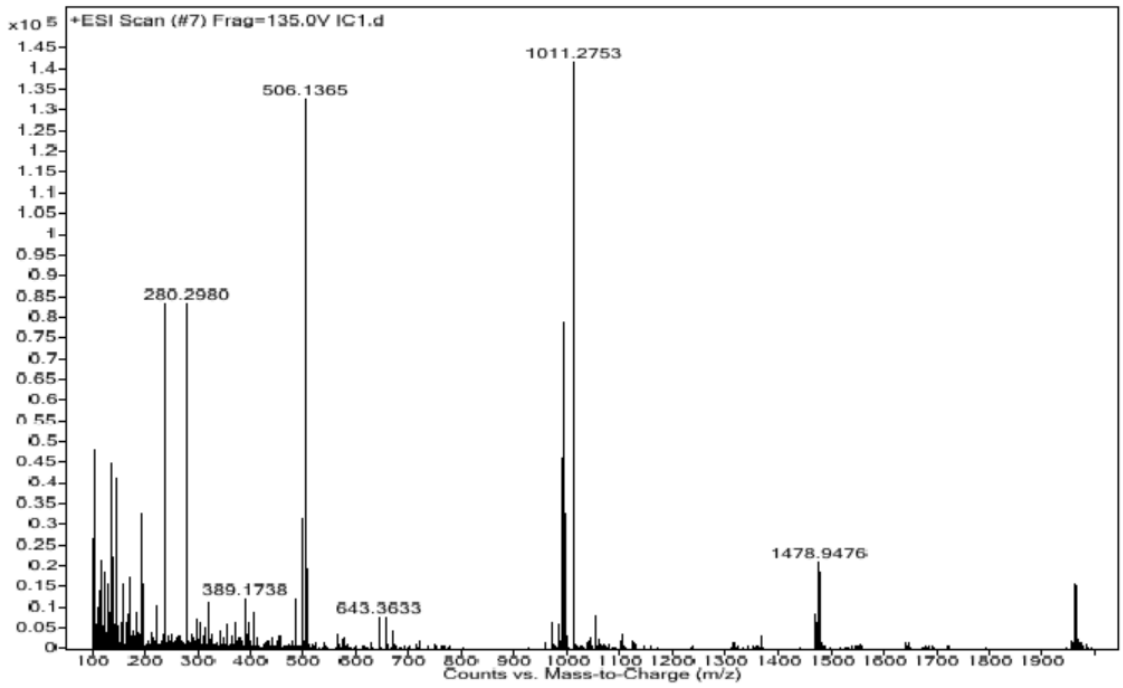

Figure 11(a). ESI mass spectra of [ALP]-α-CD inclusion complex

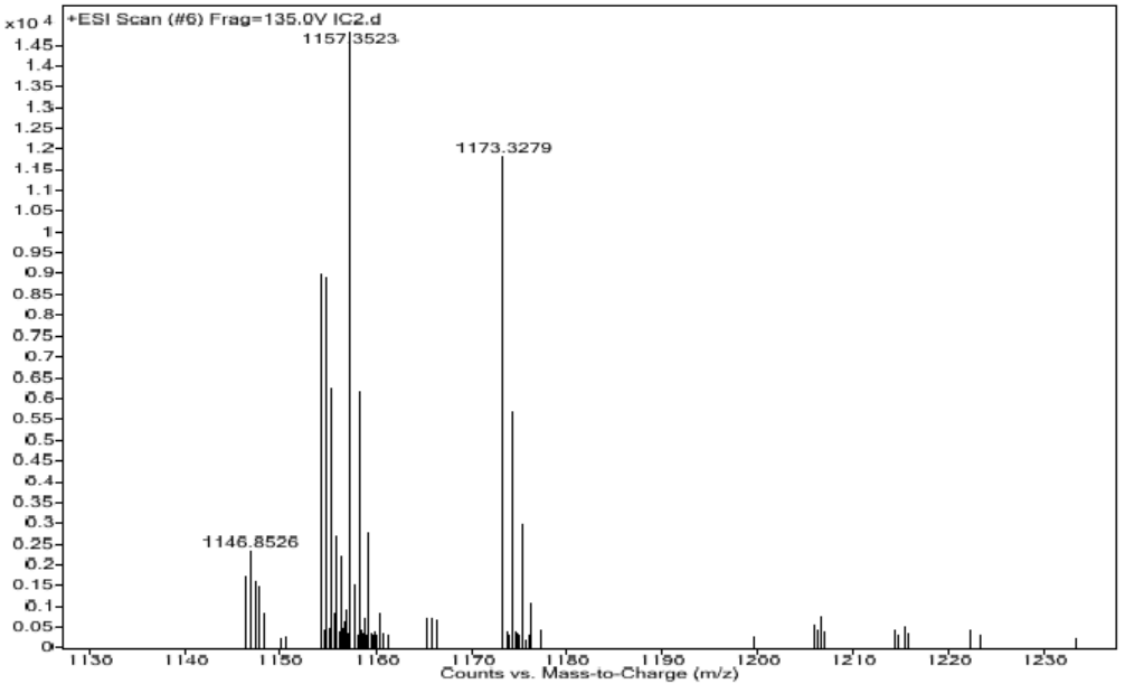

Figure 11(b). ESI mass spectra of [ALP]-β-CD inclusion complex

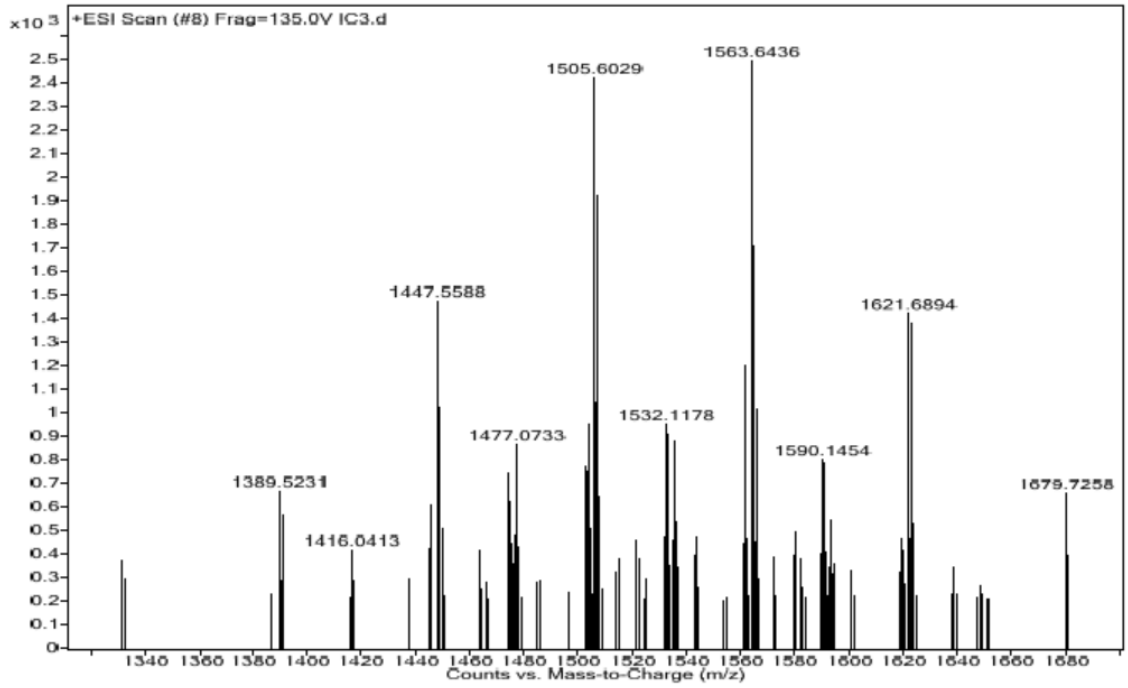

Figure 11(c). ESI mass spectra of [ALP]-HP-β-CD inclusion complex

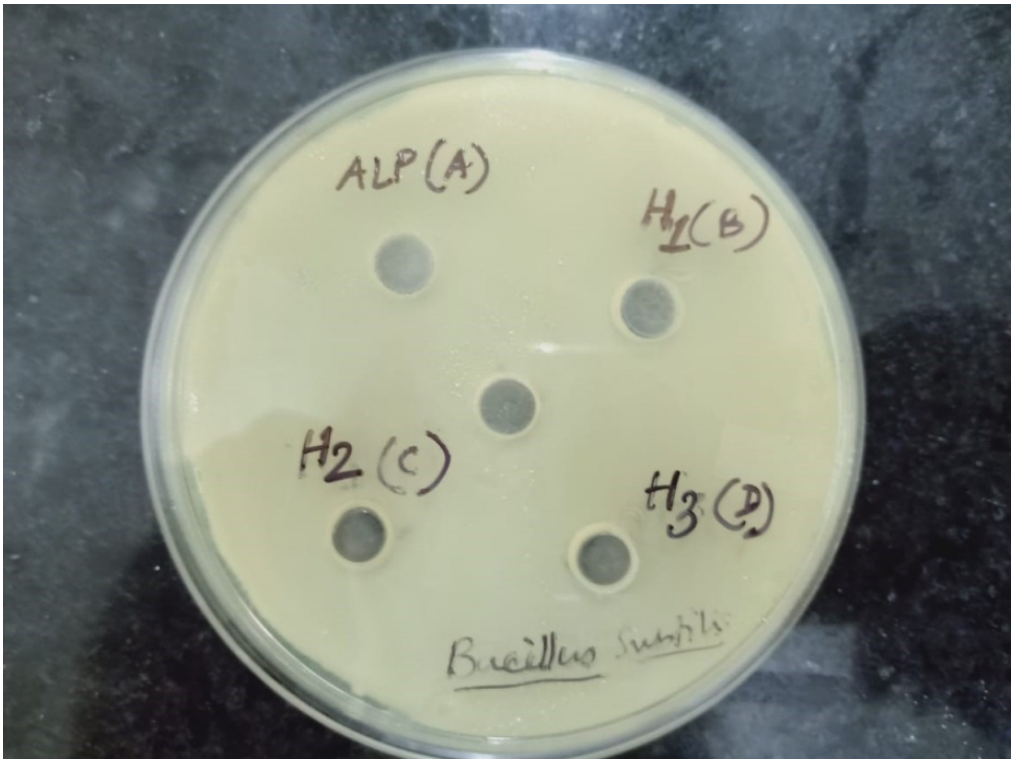

Figure 12(a). Antimicrobial activity analysis ALP on Gram-positive B. subtilis. No zone of inhibition was observed. Double distilled water was taken as the control.

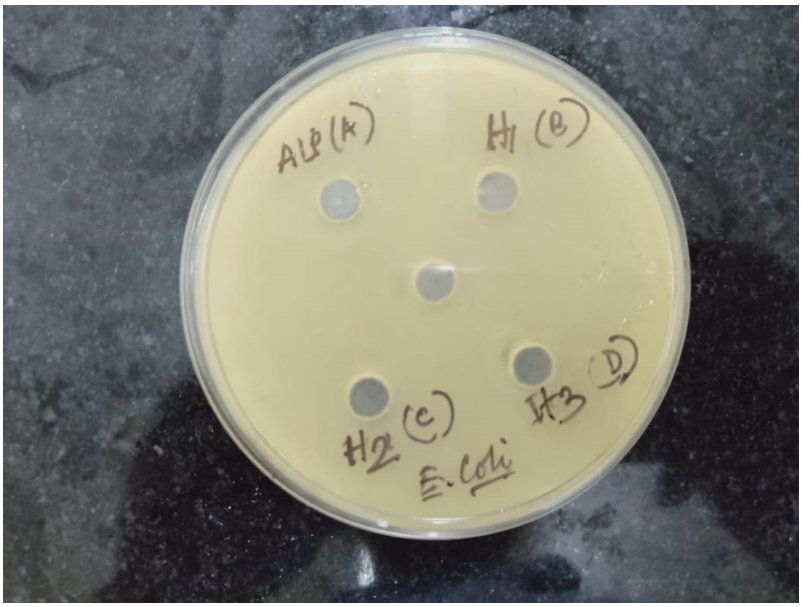

Figure 12(b). Antimicrobial activity analysis ALP on Gram-negative E. coli. No zone of inhibition was observed. Double distilled water was taken as the control.

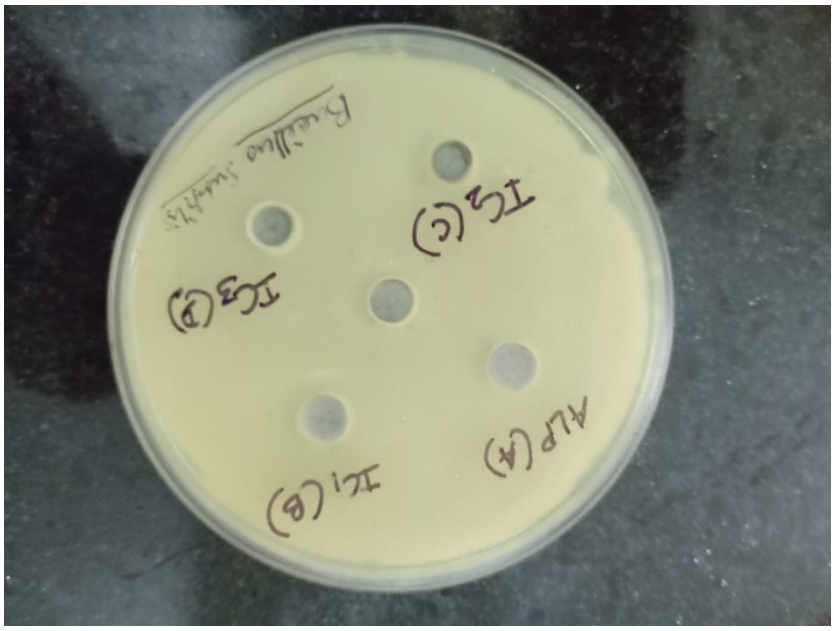

Figure 12(c). Antimicrobial activity analysis on ALP on Gram-positive B. subtilis. No zone of inhibition was observed with IC1, IC2, and IC3. Double distilled water was taken as the control.

Schemes

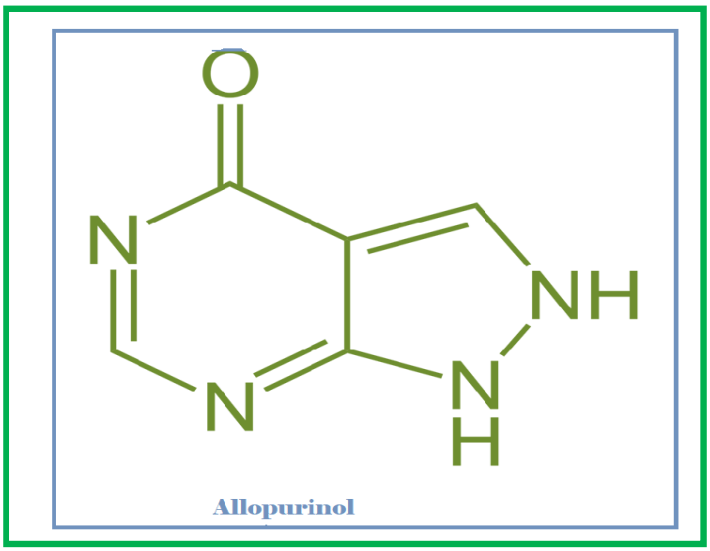

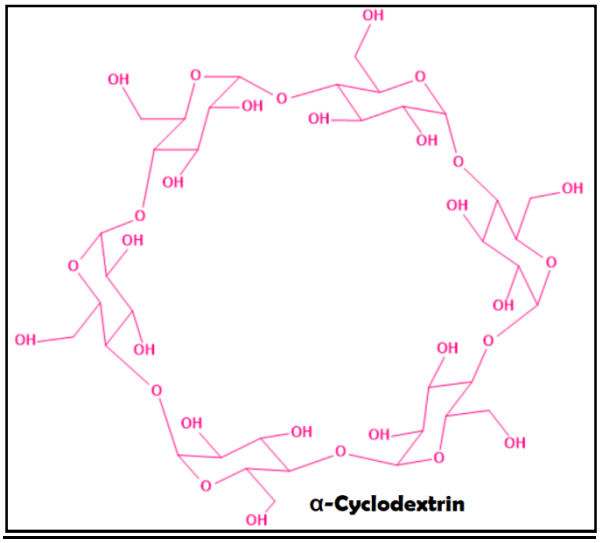

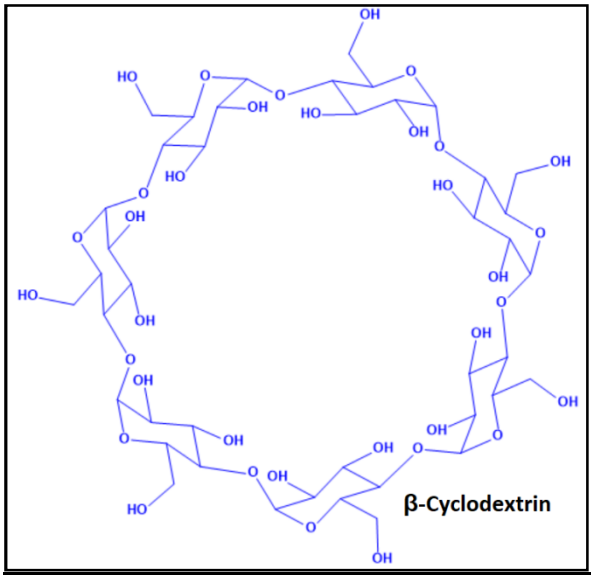

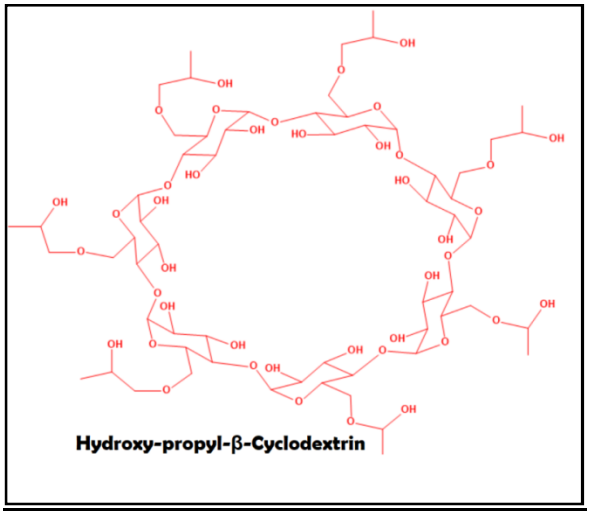

Scheme 1. Molecular Structures of the hosts and guest

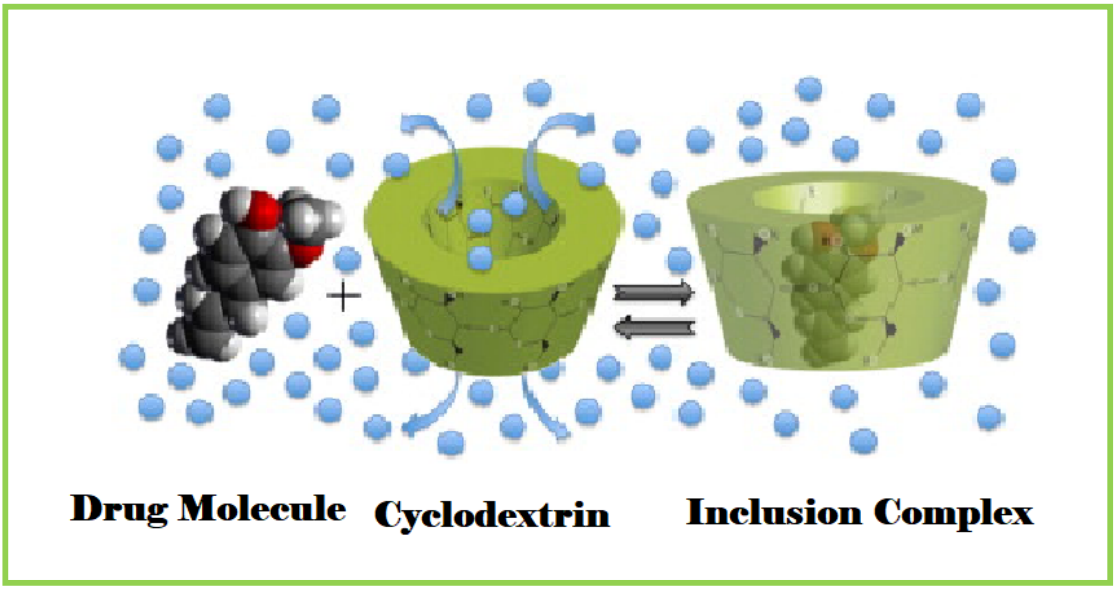

Scheme2. Diagrammatic represention of the probable complexes obtained